UCRL - 77094 Rev 1
PREPRINT

Conf-751130--3

LAWRENCE LIVERMORE LABORATORY
University of California/Livermore, California

Laser Fusion Experiments at the Lawrence Livermore Laboratory*

Harlow G. Ahlstrom

October 8, 1975

This Paper was Prepared for Submission to the APS Meeting, St. Petersburg, Florida, November 10-14, 1975.

*Work performed under the auspices of the U. S. Energy Research and Development Administration under Contract No. W 7405 ENG-48

In my talk I am going to begin with a short review of some of the important dates in the experimental fusion program at Livermore. Then I will discuss a few of the parameters of the laser systems which are being used for these experiments. I will also cover some information about specialized diagnostics which we have developed at the Livermore Laboratory for these experiments. I will also discuss the focusing arrangements for each of the systems. Finally, I will cover experiments both on planar targets and on targets for laser fusion.

VUGRAPH #1

In the first vugraph we see a listing of laser fusion experiments at the Lawrence Livermore Laboratory. In the first section we see the Janus single beam experiments which first showed evidence of compression in early December of 1974. Neutrons were produced from a glass microshell filled with deterium gas on the 19th of December. Since that time we have confirmed that the neutrons are indeed 14.1 MeV neutrons from the fusion of deterium and tritium. We have gone through a number of different target designs increasing the neutron yield from single beam experiments on Janus to 7×10^5 neutrons on the 11th of March. With a laser pulse of 18 Joules in 101 psec. At that time we modified Janus to its full two beam capability. That took approximately one month and on the 16th of April we shot a ball-on-stalk with 28 Joules in 80 psec and produced 3×10^5 neutrons. Since that time we have again investigated various target designs and increased our neutron yield on the 8th of May to eleven million neutrons using 31 Joule pulse with an 80 psec pulse length. Then on the 23rd of May we measured the alpha particle spectrum from the DT reaction, the 3.5 MeV alphas, and those measurements imply a 2 keV Maxwellian ion temperature and thus confirm that the neutrons are being produced from a thermonuclear reaction rather than a beam target reaction. We have also converted the Cyclops developmental laser into a target irradiation facility on the 25th of July and it produced 7×10^6 neutrons with a 51 Joule 80 psec pulse. That laser is

now being converted to a 2 beam operation and its ultimate capability will be 1.5 terrawatts.

VUGRAPH #2

The laser systems which have been used at the Lawrence Livermore Laboratory are first of all the Valkyrie Laser System shown in vugraph #2 which is a CO_2 laser which will produce up to 50 Joules in 1.5 nsec. Shown in the vugraph is the oscillator and preamplifier using a Lumonics gain medium and a second Lumonics amplifier as a gain medium. Then followed by two electron beam sustainer amplifiers built by Systems Science and Software followed by two large diagnostics tables for making measurements of the beam profile, the imput energy, pulse duration and etc. and finally the target chamber.

VUGRAPH #3

The third vugraph shows a photograph of the Janus System. One sees the mode locked oscillator, YAG preamplifier, rod amplifiers in this housing, two 3.5 cm clear aperture disk amplifier housings each containing six disks followed by two amplifiers with 8.5 cm clear aperture each containing six disks. The beam is then split into two beams followed by two more amplifiers in each beam of six disks each 8.5 cm clear aperture. The beam is then turned and goes into the target chamber which is shown in the next vugraph.

VUGRAPH #4

One sees the Janus target chamber, these are the vacuum housings for the lens positioners. One sees a large amount of diagnostics this is a transfer microscope for viewing the position of the target in the longitudinal and vertical direction, target positioner of the vacuum pump, etc.

VUGRAPH #5

The inside of the target chamber is shown on the next vugraph, vugraph #5, one sees the target positioner mounted on the end of the stalk where we have one of the very small 42 to 100 micron glass spheres, these are the focusing lenses for the Janus system which are 8.5 cm clear aperture f/1 lenses.

VUGRAPH #6a

This vugraph shows the Cyclops System with two of the 20 cm clear aperture amplifiers installed. VUGRAPH #6b - This system has now been converted to a target irradiation facility. Shown in this configuration with beam tubes to minimize beam stearing and air turbulence which can cause beam dedregation of the target.

VUGRAPH #7

The Cyclops target chambers is shown in vugraph #7. Beam tubes coming through the target area these are the lens manipulators for the 20 cm clear aperture f/2.5 lenses. Also shown inside of the target chamber are the x-ray pin diodes combined with K-edge filters for x-ray spectral measurements, x-ray pin diodes for measuring scattered light. Over here is the filter pack for the four channel x-ray microscope.

VUGRAPH #8

Vugraph #8 shows the Argus System which is under construction in the high bay of the office - laboratory building at Lawrence Livermore Laboratory. This laser is shown in a four beam configuration. It will have 20 cm clear aperture amplifiers. The beam will be expanded to 28 cm entering the target chamber and in its final configuration it will have a power capability of between 6 and 8 terrawatts. The funds are presently allocated for the two beam operation but money has not yet been allocated for expansion of the system to four beam capability.

VUGRAPH #9

Now I would like to discuss some diagnostics which we feel are very important to the laser fusion experiments. The first of these is shown on Vugraph #9 which is the target and beam imaging optics. In the two beam operation of Janus one sees the two focusing lenses and one sees additional diagnostics in each beam. The additional diagnostics operate in the following manner. If the target is being illuminated with the west beam then we can place a diffuser in the west beam which breaks up the coherence of the laser beam and expands the beam to fully cover the target. The east lens is used as a recollimating optic. A portion of the light coming from the west beam is reflected from a 4% reflector and then reimaged with a four meter lens onto a TV camera. This allows us then to view the target on the camera. The target can then be moved out of the way, the diffuser removed and then the same optics are used to view the intensity distribution of the west beam being focused by the west lens so that the intensity distribution, position and intensity are displayed on the TV camera. In this manner one can adjust the size of the focus energy

VUGRAPH #9 -continued-

with respect to the target and its position. In addition, we have a multiple image camera which produces a number of images of the beam at varying intensity ratios and in addition a portion of that same beam can be focused onto a streak camera. In this manner one can with the target not in place actually observe the intensity distribution at the target for a full intensity shot. Of course this can not be done with the target in place but we do observe the energy either back reflected from the east beam or forward scattered from the west beam likewise we do the same thing for the east beam.

VUGRAPH #10

The next diagnostic shown on vugraph #10a is our x-ray streak camera. The x-ray streak camera is simply an optical streak camera with the optical photocathode removed and replaced with an x-ray photocathode. This streak camera has been discussed a number of times and has now been implemented on the laser fusion experiments and vugraph 10b shows a typical trace from the x-ray streak camera. The slit of the streak camera was covered with five K-edge filters, aluminium, chlorene, titanium, cobalt and zinc and the streak camera then viewed one of the glass microsphere targets being irradiated with the Janus two beam laser. The particular data was taken with a 38.3 Joule 80 psec pulse and one sees the various energy bands resolved by the streak camera. The chlorene and titanium are probably nearly saturated. An interesting thing to note is that both the aluminium, cobalt and the zinc show a short duration peak of the x-ray spectrum which has been identified as being due to the implosion of the glass microsphere. That is the peak occurs when the microsphere implodes to its densest position near the center of the target.

VUGRAPH #11

The next diagnostic is shown in vugraph #11 and here we are conserned with accurately accounting for all the one micron energy which comes from the laser. The first part, the incident calorimeter determining how much energy comes from the laser is relatively standard as is the back scatter calorimeter which measures light collected by the focusing lens either back scatter from the west beam as an example or forward scattered from the east beam. The additional things that we have done to accurately diagnose the scattered or refracted one micron light is to place in the target chamber a series of some 30 silicon pin diodes with one micron filters in front of them. These have been calibrated and allow us to map the scattered or refracted light energy inside the target chamber which is not collected by the focusing lens. In addition, we used a splitter to examine the light which is collected by the east lens with a series of photodiodes to map the intensity distribution that is measured by the scattered calorimeter.

VUGRAPH #12

Vugraph #12 shows an other example how we can account for the light which is not collected by the focusing lenses. This is a one micron box calorimeter, one sees holes which allow the focused light to enter the calorimeter and irradiate the target. There is an additional small hole at the top for the target positioner to go through. There are two holes 90^{0} to the beam in the horizontal direction, one for the optical transfer microscope for longitudinal referencing of the target and another for the x-ray microscope and a small hole in the bottom of the box calorimeter to allow one of the x-ray spectrometers to view the target. With this calorimeter we block the ions from hitting the calorimeter surface with a glass plate which passes

VUGRAPH #12 -continued-

the one micron radiation so the calorimeter only measures the one micron radiation and with this calorimeter we are able to account for 90% including the lenses, of the total solid angle.

VUGRAPH #13

In addition, vugraph #13 shows another method of accounting for the energy which is absorbed by the target. It is a differential calorimeter which measures both the one micron light and all of the ion energy which is produced in the expanding plasma. It is a differential calorimeter the central portion measures both the one micron light and the ion energy, the outer portion which is balanced in area with the central portion measures the one micron light only because the ions are stopped by the glass plate. This calorimeter is used to measure the ion energy and by assuming a distribution of ions one can calculate the total energy which was absorbed by the target.

VUGRAPH #14

This vugraph shows a schematic of the four channel x-ray microscope which is used to image the spatial distribution of x-rays from the laser fusion targets. We have schematically a laser fusion target, a k-edge filter pack with four filters for the four channels and we have the crossed cylindrical grazing incidence mirrors which produce the four images in the film plane. In the microscope which is used, this mirror is coated with nickel, these two mirrors are coated with nickel in this region and are bare glass in this region and this mirror is bare glass so that we have two channels which use glass mirrors and two channels which use nickel mirrors.

VUGRAPH #15

This vugraph shows two stainless steel wire meshes which were back lighted with a Henke tube and focused with the x-ray microscope. One sees the 25 micron spacing of the wires in the mesh and the characteristic 8 microns thickness of the wires in the mesh.

VUGRAPH #16

Vugraph #16 shows several densitometer traces of this vugraph and one can see the 25 micron spacing at this point and as one looks at the angles between the wires coming together one can see that at this point one can resolve as small a dimension as three microns. Indicating that the best resolution or the resolution at the center of the field of view of this microscope is three micron.

VUGRAPH #17a

In this vugraph we show the type of microscope which has been designed as an improvement over the simple two cylindrical lens microscope. This one involves the use of a hyperboloidal mirror as the first reflecting surface and an ellipsoidal mirror as the second reflecting surface and the system is axially symmetric. This produces a typical increase in collecting solid angle for the microscope of at least a thousand and possibly even ten thousand over the simple microscope and its other advantage is its inherent higher resolution. The calculated resolution of this type of microscope is shown on vugraph 17b.

VUGRAPH 17b

This vugraph shows where we plot the calculated resolution in the object plane in microns as a function of off axis position of the image. Since the microscope is made up of conic sections it has a infinite theoretical

VUGRAPH 17b-continued

resolution on axis and is degraded as one goes off axis. One sees that for an off axis position of up to 220 microns, one still has a resolution of 1 micron referenced to the object plane. In actual fact the resolution will be limited by manufacturing tolerances and we expect to obtain a resolution somewhat better than a micron but certainly approaching diffraction limited operation.

VUGRAPH #18

Vugraph #18 shows the Valkyrie focusing system, we have a f/2 NaCl lens which is used to focus the beam onto the target. In addition, we have another f/2 lens which is used as a recollimating optic for viewing the intensity distribution as was done on the Janus system.

VUGRAPH #19

Vugraph #19 shows the beam profile which is obtained with the Valkyrie laser. The upper trace shows the near field pattern at the focusing lens which shows a very nice Gaussian distribution of intensity and then the lower trace is an intensity distribution at the focus for the Valkyrie System and again one sees a very nice gaussian distribution with a FWHM of approximately 70 microns.

VUGRAPH #20

This vugraph shows the focusing system for the Janus laser. The thing to note in this viewgraph is the lens positioners which have three translation stages and two rotation stages which allow the manipulation of the lenses under vacuum with a resolution of 0.4 micron.

VUGRAPH #21a

The next vugraph shows the beam profile which is produced by one of the Janus laser beams. This is the east beam at 184 gigawatts and what we are looking at is the intensity distribution at various points approaching the best focus of the beam. In this direction we are moving approximately 30 microns in longitudinal position and in this direction we are changing the intensity on the film by a factor of two. This is done with a multiple image camera and the viewing system which was discussed earlier. These regions are typically the size of the targets which are used for the laser fusion experiments and one can see some structure in the beam but basically a relatively clean focused beam.

VUGRAPH #21b

This vugraph shows energy contours of these photographs where they have been processed with a densitometer and a program to change film density into intensity and one sees the lower power intensity distribution and the comparison with the high power intensity distribution showing the affect of the whole beam self focusing producing a donut shaped intensity pattern at the target.

VUGRAPH #22

Vugraph #22 shows the focusing system which is now being implemented on Janus. It is an ellipsoidal mirror focusing system with low f # lenses similar to the system used at the KMSF Laboratory. This system consists of two eccentricity 1/3 ellipsoids and two sets of low f # lenses. In our particular case we went to a doublet design to reduce the difficulty of making lenses and and the severe Frenel reflection losses which would occur had we made a single element f/.47 lens.

VUGRAPH #23

vugraph #23 shows the calculated intensity distribution which will be produced at the target using the Janus beam profile which is super Gaussian profile with the exponent to the fifth power. One sees that we will improve the intensity distribution to ± 30% variation in intensity over the surface of the target and in addition the maximum deviation of the angle of the rays from normality at the surface of the target will be 15°. (VUGRAPH #24) The Cyclops system uses 20 cm clear aperture lenses and in this case the lenses are outside the target chamber and the intensity is focused through fused quartz windows. (VUGRAPH #25) These are f/2.5 lenses. The Argus System will use an ellipsoidal mirror system too, but substantially different than Janus, almost a factor of 2 larger in diameter but in addition we have done something else to improve the system and that is recognition that the small scale beam break up is affected by all glass that is in the laser path. If we were to make the same system as we did on Janus then the thickness of the lenses would be increased by a factor of 2 over what we show here and that would have significantly degraded the focusable energy that we would be able to produce with Argus. In this case we have added a second ellipsoidal mirror and a reflecting surface on the back of the inner ellipsoidal mirror which allows us to go to a doublet which is equivalent to f/1.2 lens instead of a f/.47 lens. This system is under construction and will be used with Argus. The intensity distribution which we expect to produce is shown on vugraph #26.

VUGRAPH #26

One notices the very high degree of uniformity and the very small deviation from the normality of the rays on vugraph #26. Of course, at this point this is a calculated distribution and not a measured distribution.

VUGRAPH #27

Now I would like to move on to the laser experiments. We have done experiments on the Valkyrie laser at 10.6 microns using both thin foils and disk targets. The experiments were conducted with a pulse length from 1 - 3 nsec and a laser energy from 10 - 30 Joules which focused on the target then produced an intensity range of from 10^{13} - 10^{14} watts per cm^2. The important results from these experiments were the relatively cool plasmas which were produced with this intensity which is attributed to the refraction of the light by the plasma and as a result compared to an equivalent experiment at 1 micron we saw that the extent of the plasma compared to the focal region was significantly larger and as a result since more plasma was heated the plasma was simply cooler. In addition we observed in these experiments evidence of localized plasma heating which could be filamentation of plasma which was observed using x-ray pinhole cameras and as such could be either due to x-ray emitting regions or due to electron.

VUGRAPH #28

Vugraph #28 shows the x-ray pinhole pictures and the first image is with a 5 micron polyethylene foil. One sees the bright spots which could be due to intense x-ray emitting regions or intense electron emitting regions. This phenomenum was also observed in the disk experiments with 5 micron thick by 120 micron diameter parylene disks. Again one observes filamentation due to intense x-ray emitting regions or electrons.

VUGRAPH #29

This vugraph shows the plasma expansion and acceleration. The first views are for a polyethylene foil and because of the target holder one only

VUGRAPH #29-continued

sees the plasma blow off region at two intensity values. The second set of images shows the streak images of the parylene disk experiment and here one can see both the plasma blow off and the acceleration of the back surface which is very low due to the very poor coupling of the energy to the parylene disk. (VUGRAPH #30a) Experiments similar to these have also been done on the Janus system at one micron and here the laser was operated at approximately 5 - 10 Joules with pulse length of between 60 - 100 psec with an intensity varying from 10^{15} - 10^{16} w/cm^2. In these experiments we have observed an absorbtion of only 15 to 25%. The diagnostics described previously were used to measure the angular distribution of the backscattered laser energy and it was shown that it is highly peaked in the back scatter direction. In addition, with the streak camera in the diagnostics system we were also able to measure the time dependence of the back reflection and the experiments show that as the intensity in the experiments increased the back reflection exhibited was an intensity different from distribution from the laser. Also the x-ray spectrum is measured and it is quite obvious that the high energy portion of the x-ray spectrum is related to the intensity distribution at the target. In addition the x-ray microscope pictures were used to determine the scale length of the plasma and it has been shown that the scale length in the direction of the laser is approximately 10 microns. With the lateral dimension of the plasma being determined by the input intensity distribution.

VUGRAPH #30b

This vugraph shows the angular distribution of the light which is reflected or scattered or refracted from the plasma and in the direction that the laser is coming from one sees a very highly peaked distribution. Coming back towards the laser in this direction is the light which goes around the target. The two experiments which are shown here were at approximately 6 Joules with 60 - 70 psec and the fraction of energy absorbed was 15% for the low intensity and 19% for the high intensity shot. The intensity was changed by changing the focusing from 90 microns down to 30 microns.

VUGRAPH #31

The x-ray spectrum is shown on vugraph #31. Here we are showing the spectrum of the x-rays from first the low energy portion of the spectrum. One sees that the low energy portion of the spectrum is not significantly changed however when one gets above 20 kilovolts one sees a very strong dependence on intensity. The much harder spectrum occuring at the higher intensity. These experiments have been shot a number of times and for the same intensity one can reproduce the x-ray spectrum within about 10%.

VUGRAPH #32a

This vugraph shows the electron spectra which is measured with a magnetic spectrometer and the first part of the vugraph shows the distribution function in electrons per keV vs the energy and again one sees that the distribution and number of high energy electrons which are emitted from the target are stronly dependent on the intensity of the laser focus. The second part is a energy distribution keV per keV as a function of keV.

VUGRAPH #32b

We have also used the streak camera as shown in figure 32b. We show the distribution of the light which is incident on the target in time and the distribution of the back reflected light which is recorded by the streak camera looking through the focusing lens. At low power, 10^{15} w/cm^2 we do not see any difference in the time dependence of the incident reflected pulse. However, at 10^{16} w/cm^2 we see what could be characterized as a saturation effect of some of the light coming back through the lens.

VUGRAPH #33

This vugraph shows a plot of the yield ratio that is fusion energy compared to the laser light energy into the target as a function of laser aperture. Over on the left we see the Janus 1 experiments and the calculations for the type of target which is now being used which we call an exploding pusher target or high entropy change shock compressed target. Janus 2 data is also shown here and the calculations. Cyclops calculations - the best that we expect to do on Cyclops is shown by this point. On the Argus System shows that when we get to Argus with the four beam system we expect to be doing experiments with high density type targets that is targets which are nearly isentropically compressed.

VUGRAPH #34

One of our target designs is called the ball-on-plate and is shown on vugraph #34 and is simply a glass plate with the glass microshell filled with DT glued to the plate.

VUGRAPH #35

Vugraph #35 is an engineering drawing of the target shown on vugraph #34. Also shown here is the technique for irradiating the target. It has been used with Janus in single beam configuration and one sees the beam being focused down onto the ball and part of the energy going onto the plate. The purpose of the plate is to provide additional plasma to allow thermal conduction by the electrons to carry energy around to the back of the target and to cause the back of the target to implode as well as the front of the target. An experiment which was done with this target was 15 Joules 90 psec gaussian pulse where 3.6 Joules were absorbed with a neutron yield of 1.1×10^4 and the calculated compression and temperatures were - a compression of 50 an ion temperature of 700 eV and electron temperature of 350 eV.

VUGRAPH #36

This vugraph shows the x-ray spectrum of this target both the measured and calculated and shows the non Boltzmann distribution of the high energy x-rays.

VUGRAPH #37

The next vugraph shows a x-ray microscope picture of the target taken in the 1.5 keV range. The picture has been densitometered and been color enhanced. One sees here the position of the glass plate, the original position of the glass microshell and the imploded configuration producing the high intensity x-rays when the walls of the glass shell implode and heat to high temperature.

VUGRAPH #38

The next vugraph shows what can happen if the focusing is not done correctly. In this case the focus was opened up to approximately 100 microns and so a great deal of the energy was incident on the glass plate and as a result the glass plate was heated to a high temperature but the target - the fuel ball stayed relatively cool and one does not see a central compression region and in the experiment no neutrons were observed.

VUGRAPH #39

The next class of target, shown on vugraph #39, is called ball-in-plate target and it is simply a two beam version of the target shown previously. The plate now is placed at the equator of the ball with respect to the beams coming into the target.

VUGRAPH #40

Vugraph #40 shows an engineering drawing for vugraph #39. It shows a small angular gap between the plate and the glass shell. In this experiment we had approximately 28 Joules absorbing 9 Joules the number of neutrons produced was 5×10^5. The calculated ion temperature was 1.5 keV and the electron temperature was 700 eV and a compression of 80 was calculated for the experiment.

VUGRAPH #41

This vugraph shows the calculated and measured x-ray spectrum, again showing the good agreement that is obtained between the calculations and the experiment.

VUGRAPH #42

This vugraph shows the x-ray micrograph of this target - first in the 800 eV channel of the x-ray microscope and now one observes the initial position of the target and the illumination where the energy was initially absorbed, one sees the imploded region and one also sees the plate and since ore is viewing in a side view and the plate did not get as hot as the rest of the target one sees this particular channel in absorbtion. Indicating that there are probably some very interesting spectroscopy that could be done with these types of targets.

VUGRAPH #43

This vugraph shows the same target with the 2.5 keV channel of the x-ray microscope and now we see very little emission from the initial position of the glass shell. We see the bright emission from the tight hot core of the central portion of the target as it imploded.

VUGRAPH #44a

This vugraph is a summary of experiments with the ball-on-stalk target that is simply a glass microshell filled with DT radiated with the two beams from the Janus system. The purpose of this set of experiments was to examine the affects of fill density on the neutron yield and implosion of the target. And also on the effects of simultaniety of the beam. In setting up the Janus system we have referenced a position which we believe is approximately 3 - 5 psec of where the two beams arrive simultaneously. So as we examine this vugraph #44 we see the summary laser conditions, the beam energy in the west beam and the east beam and the energy which was absorbed by the target, the pulse length in psec, the mass of the target, the diameter of the target, the wall thickness, the fill and milligrams per cubic centimeter, simultaniety of the beams, the neutron yield,

VUGRAPH #44a-continued-

ion temperature inferred from the alpha spectrometer, the electron temperature from the thermal portion of the x-ray spectrum and the exponential term which would describe the high energy portion of the x-ray spectrum. What we have observed is that experiments with zero fill indicate no neutron yield, ½ milligram, 2, 3, 5, and 8 milligrams and the neutron yield for those experiments peaking at about 3 milligrams per cubic centimeter. In addition we see the affect of target size in the neutron yield peaking at approximately 80 micron diameter target and finally the effect of beam simultaniety. The neutron yield being 2×10^6 vs simultaneous beams dropping to 5×10^5 for 42 picosecond delay for one of the beams and dropping further to 7.5×10^4 for 94 picoseconds and finally dropping to 25,000 when one of the beams did not arrive at all.

VUGRAPH #44b

This vugraph shows the distribution of the 1.06 um light refracted and scattered by the target for two planes - ll and l to the plane of polarization of the incident radiation. The lower values for the plane ll to the incident polarization may well be evidence of resonance absorption.

VUGRAPH #45a

This vugraph shows the various x-ray spectra which are obtained from the experiments for the variation in target size.

VUGRAPH #45b

This vugraph shows that the superthermal x-rays decrease as the beam delay increases.

VUGRAPH #45c

This vugraph shows the Lagrangian mesh of a LASNEX calculation of the ball-on-stalk target for 2 mg/cm^3. The dotted line shows the glass-DT interface of peak fuel density.

VUGRAPH #46a

This vugraph shows the x-ray microscope picture for the target which had zero fill and produced zero neutrons. One sees a very intense structure at the center because of the total collapse of the silicon dioxide as it was imploded.

VUGRAPH #46b

This vugraph shows the target with a half a milligram fill and shows a small reduction in the intense portion in the center of the target.

VUGRAPH #46c

This vugraph shows an x-ray micrograph of the target with two milligram fill and now you can see that the central region has expanded considerably, the volume compression is reduced by the increased fuel mass but we still get a significant implosion of the target.

VUGRAPH #46d

And now we go to five milligrams and the effect becomes rather dramatic. For now we see that the silicon dioxide did not pass all the way across the center and there is a significant reduction of the volume compression of the target.

VUGRAPH #46e

And now we go to 8 milligrams per cubic centimeter and now you see the volume reduction is reduced even further.

VUGRAPH #47a

This vugraph shows a 2 milligram fill target with the simultaneous beam arrival. Vugraph #47b now shows the dramatic affect of delaying one beam with respect to the other. In this case the beam from the right was unchanged the beam from the left - the east beam - was delayed by 42 picoseconds and you can see bright central region has moved significantly to the left and this structure in the central region probably indicates a jetting of the early arriving portion of the implosion. Vugraph 47c And now we have delayed the beam on the left 92 picoseconds and the jetting and very asymmetric implosion has shifted even further to the left. Finally the beam from the left in Vugraph 47d just never arrived and one can see very asymmetric character of the implosion. The right side of the shell was simply driven over towards the left and a small number

VUGRAPH #47d-continued

of neutrons were produced.

VUGRAPH #48a

This vugraph is a reduction of some of this x-ray microscope data which shows the x-ray spectrum from one of the ball targets. Taken with the silicon PIN diodes and filters and the lead stearate crystal spectrometer and a RAP crystal spectrometer. Plotted with this we have also shown four points on the x-ray spectra determined with the four channels of the x-ray microscope. One for the total target - these four points and secondly for the compressed core region showing these four points. This is where we are trying to go with the x-ray microscope - to actually get spectral information out of it and later to couple it to the x-ray streak camera and get both spatial, temporal and spectral information out of the x-ray microscope.

VUGRAPH #48b

This vugraph shows a plot of the number of neutrons produced per Joule of absorbed laser energy as a function of the Joules of absorbed energy divided by the number of nanograms of the target. The importance of this is that if more laser Joules into a particular mass of target the target area gets hotter and the ion temperature rising rapidly gives a rapid rise of the neutron yield because of the rapid rise in the $\langle \sigma v \rangle$. The The data shown here shows about a power dependence of approximately four for these type of targets.

The final subject I wish to discuss is the alpha time of flight spectrometer for measuring energy distribution of 3.5 meV alphas. VUGRAPH #49 shows a schematic of the experiment. One simply has a time of flight tube and a magnet to bend the alphas out of the line of sight onto a Flour photomultiplier

VUGRAPH #49

combination. The x-rays and electrons and everything else continue along the line of sight and are dissapated in a get lost tube. This technique allows us to measure the energy distribution of the alphas with a yield level of only 10^6 and resolve 100 kilovolts. This measurement is intended to be made for neutrons as well but because the neutrons are four times faster and four times less massive it turns out that a yield level of 10^8 is required to make the measurement that was made with the alphas.

VUGRAPH #50

This vugraph shows the experimental data which shows the ion temperature of the experiments as a function of the energy spread of the alphas FWHM energy spread. There are a number of experimental points representing different experiments. I should comment that these points had not been corrected for the additional broadening caused by the passage of the α's through the fuel or through the pusher or the Doppler broadening due to the thermonuclear burn occuring while the fuel is being imploded. Several comments are in order we have a number of experiments which uncorrected temperatures from about 1.8 keV up to about 6 keV. This point seems rather anomalously high because of the alpha distribution measured by the photomultiplier was a double peaked distribution and there are a number of possible explanations why it was double peaked but we have simply included the FWHM of the distribution.
The point at 10 keV is probably not a real thermonuclear burn, possibly some beam target neutrons and alphas were produced. The target had a large prepulse something like 300-400 microjoules of prepulse that got to the target before the main laser pulse arrived and it is our experience that above 100 microjoules the target is generally disassembled - that is the glass shell is

VUGRAPH #50

shattered by the prepulse before the main pulse arrives. DT gas could have been in the plasma corona for this particular target.

VUGRAPH #51

Here we show the calculated energy loss of the α's for two pusher models, exploding and ablation compressed. The energy loss in the experiments 200-300 keV is consistent with :

1) The reactions occurring in the compressed core
2) The exploding pusher type of implosion
3) LASNEX calculations of compressions of 70-100
4) x-ray microscope photos of the geometry of the implosion
5) the reactions being TN reactions

In summary, we have at the Lawrence Livermore Laboratory three laser systems which has been used for laser fusion experiments, Valkyrie, CO_2 Laser, two beam Janus System and the single beam, Cyclops Laser. In six to nine months we expect to be operating the two beam Argus System. We have done a large number of experiments which confirm that glass microshells filled with DT can be imploded and we have confirmed that we can produce neutrons and that they are indeed thermonuclear neutrons and more importantly we have been able to calculate these targets and calculate the observables which are measured by our diagnostics.

CUMULATIVE LASER FUSION EXPERIMENTS — LLL

JANUS single beam

12/6/74 — First evidence of compression
12/19/74 — 1.2×10^4 neutrons, 15 J, 100 psec
1/3/75 — Time of flight information implies 14 MeV neutrons
1/30/75 — 2×10^5 neutrons, 16 J, 100 psec
2/26/75 — Ball-on-plate yields 1×10^4, 15 J, 100 psec
3/11/75 — 7×10^5 neutrons, 18 J, 101 psec

JANUS two beam

4/16/75 — 3×10^5 neutrons, ball-on-stalk, 23 J, 80 psec
4/18/75 — 2.3×10^6 neutrons, 27 J, 80 psec
4/29/75 — 8×10^5 neutrons, ball-on-stalk
4/25/75 — 5×10^6 neutrons
5/8/75 — 1.1×10^7 neutrons, 31 J, 80 psec
5/23/75 — α particle spectrum implies thermal origin of neutrons. 2 keV Maxwellian ion spectrum.

CYCLOPS single beam

7/25/75 — 7×10^6 neutrons, 51 J, 80 psec
8/14/75 - 1.2×10^7 neutrons, 68 J, 80 psec

Artist: Please update as indicated.

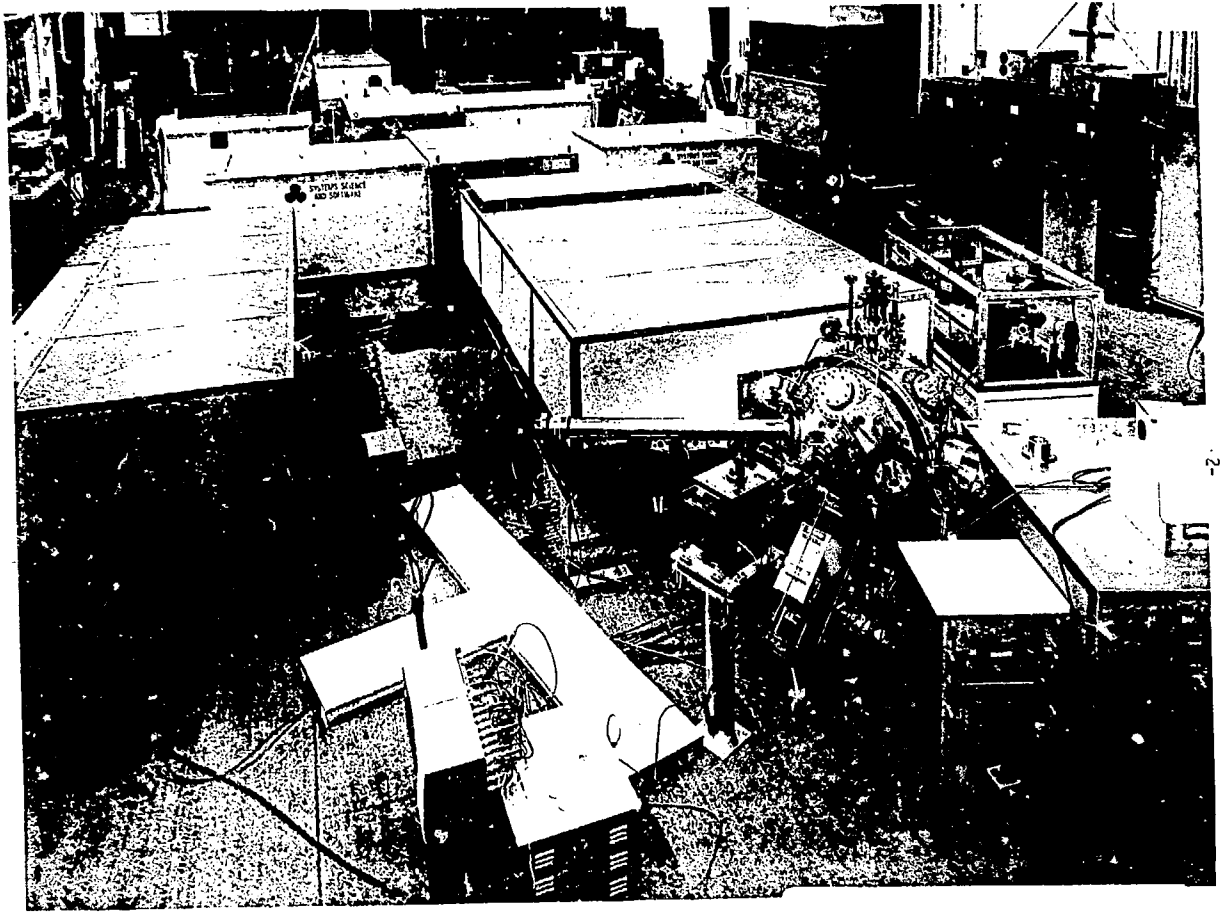

06-300475-0380

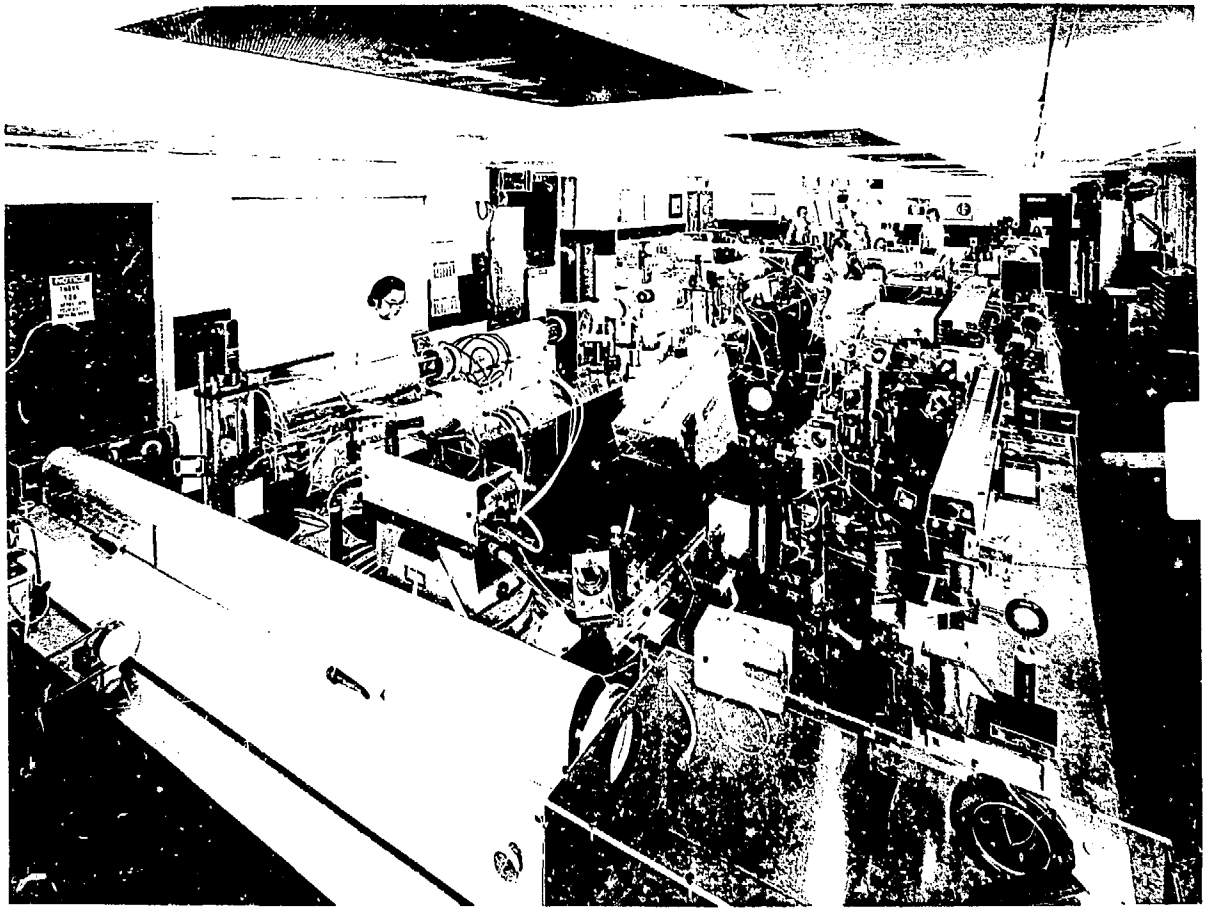

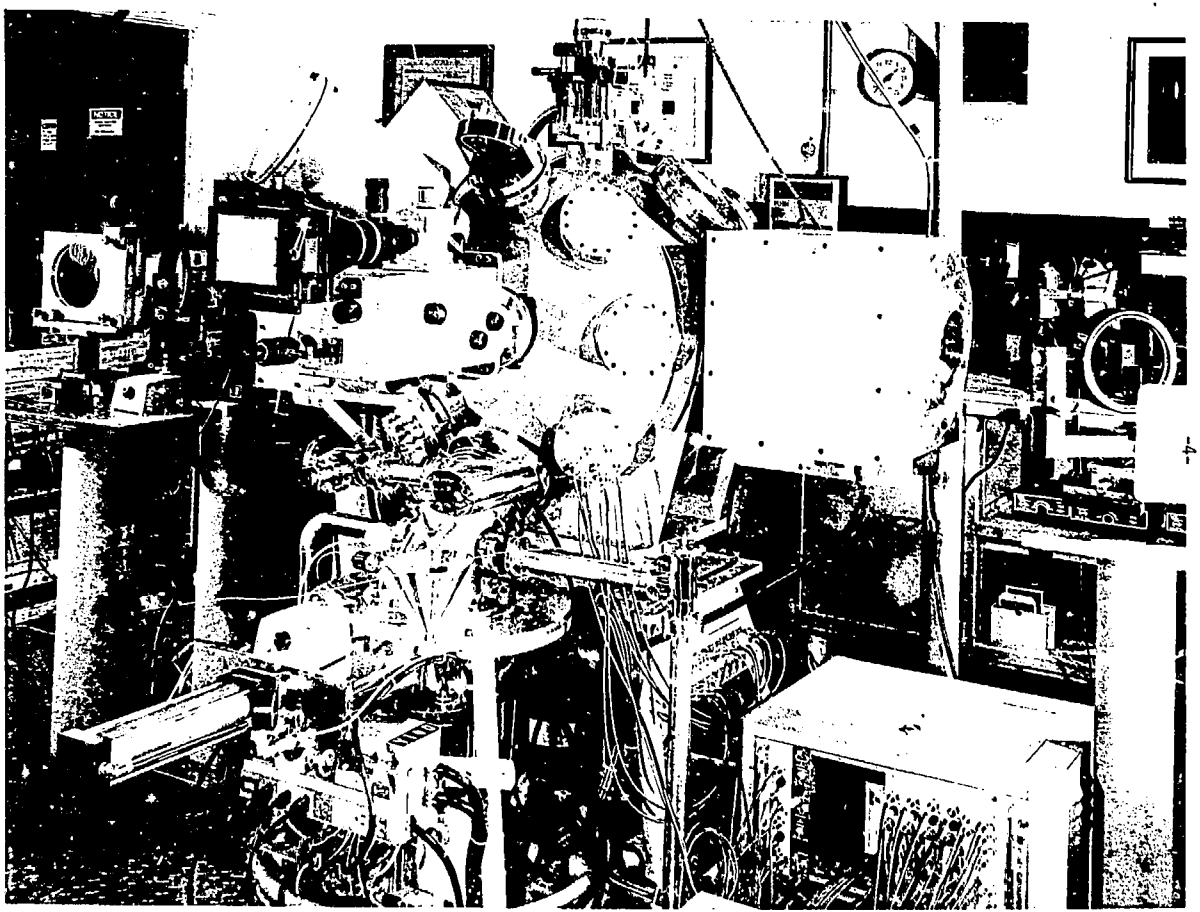

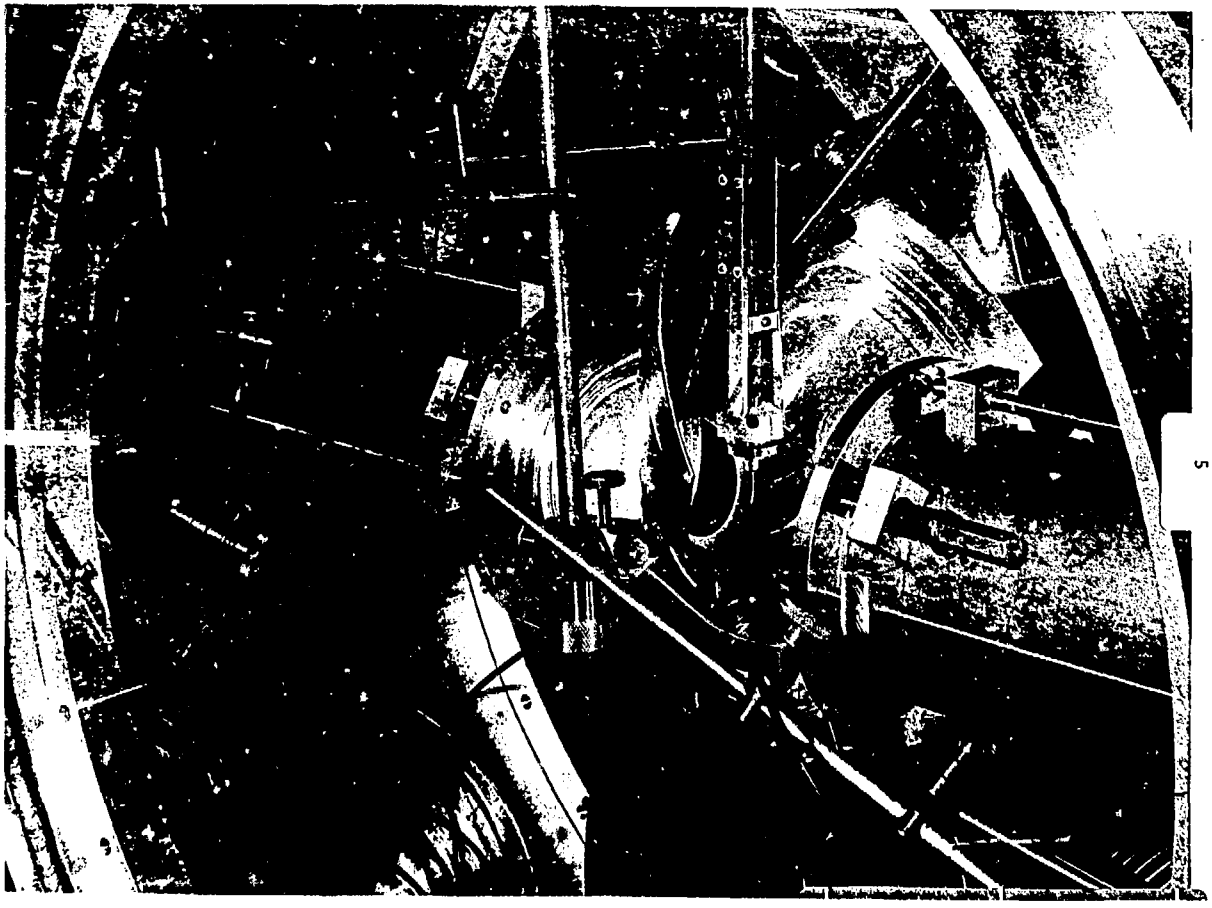

02-26-0175-0024

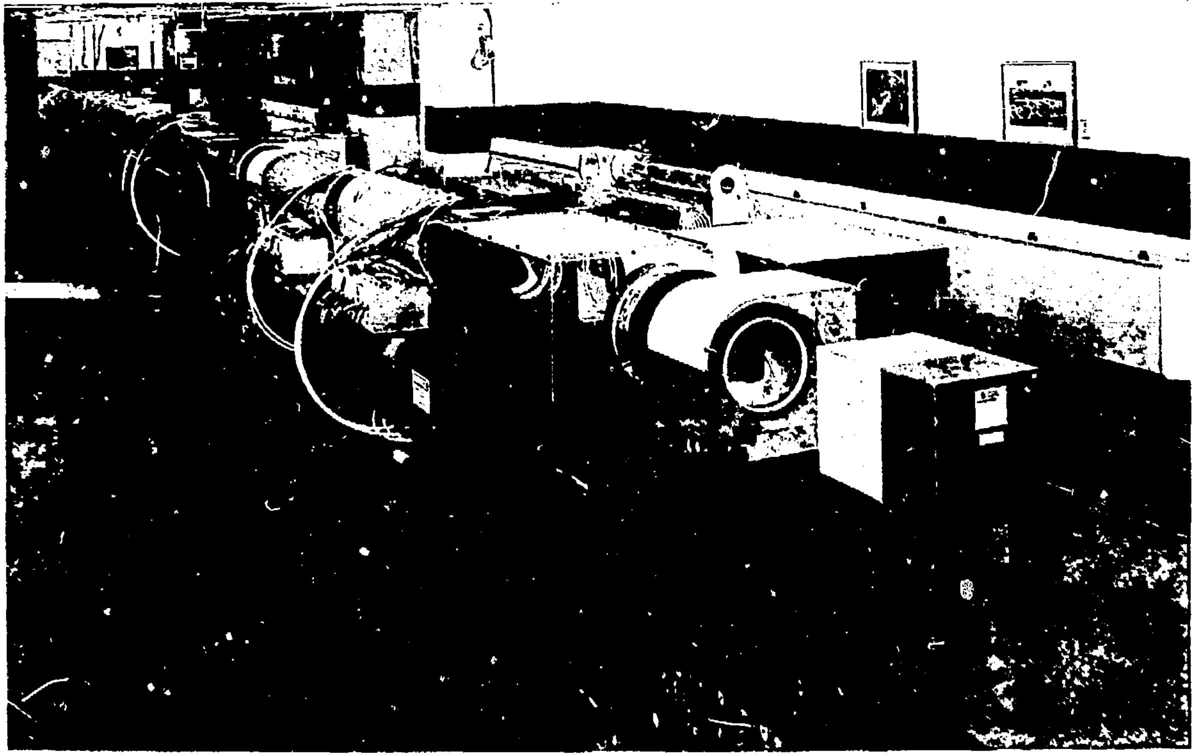

(a)

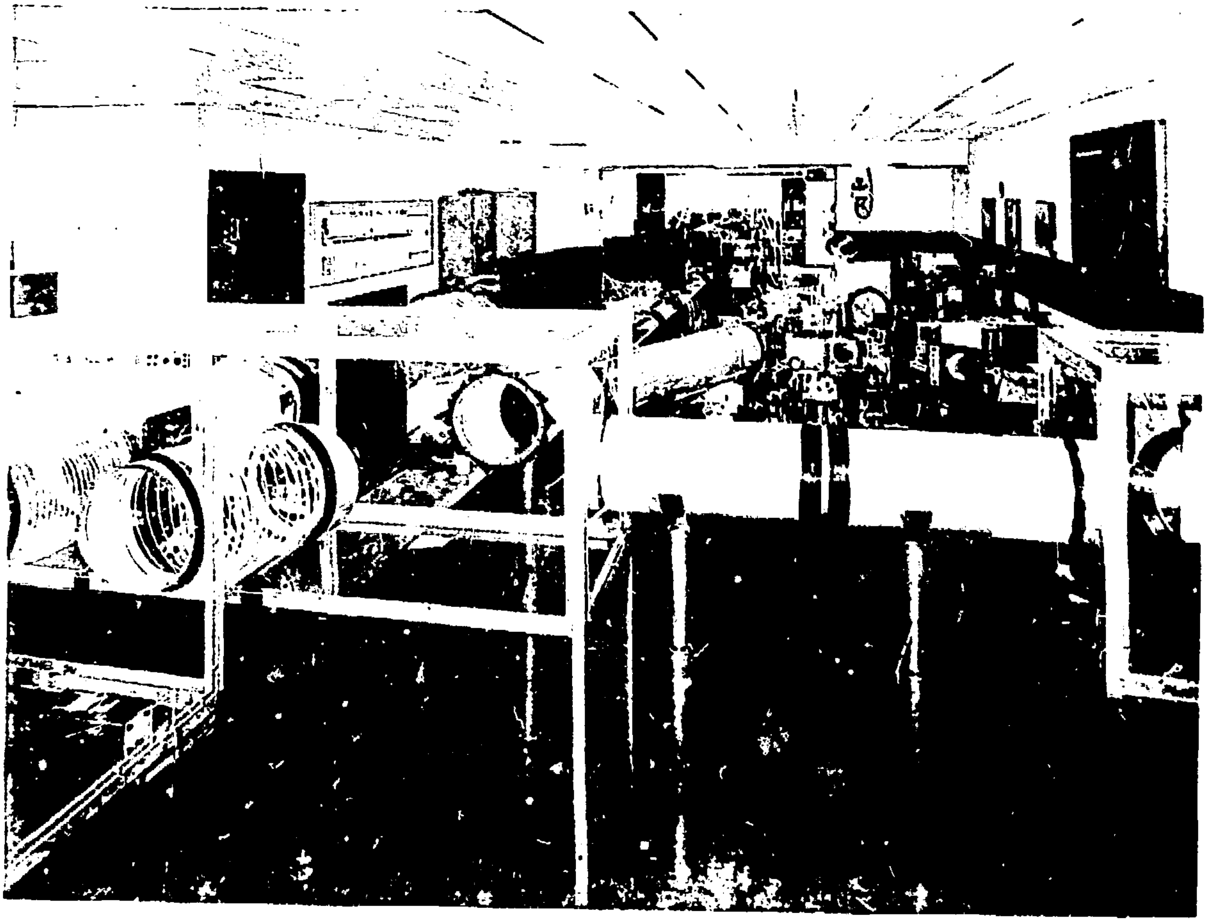

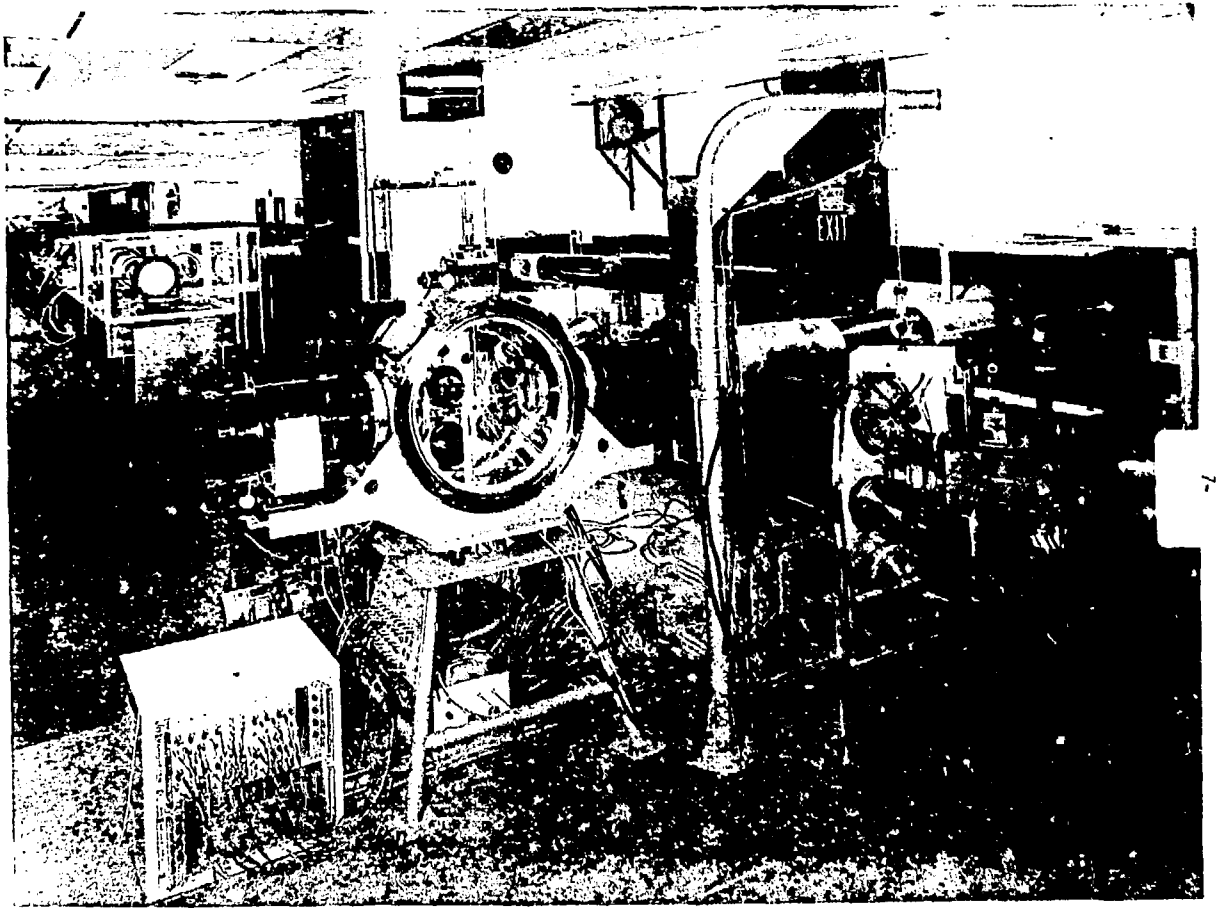
EXIT

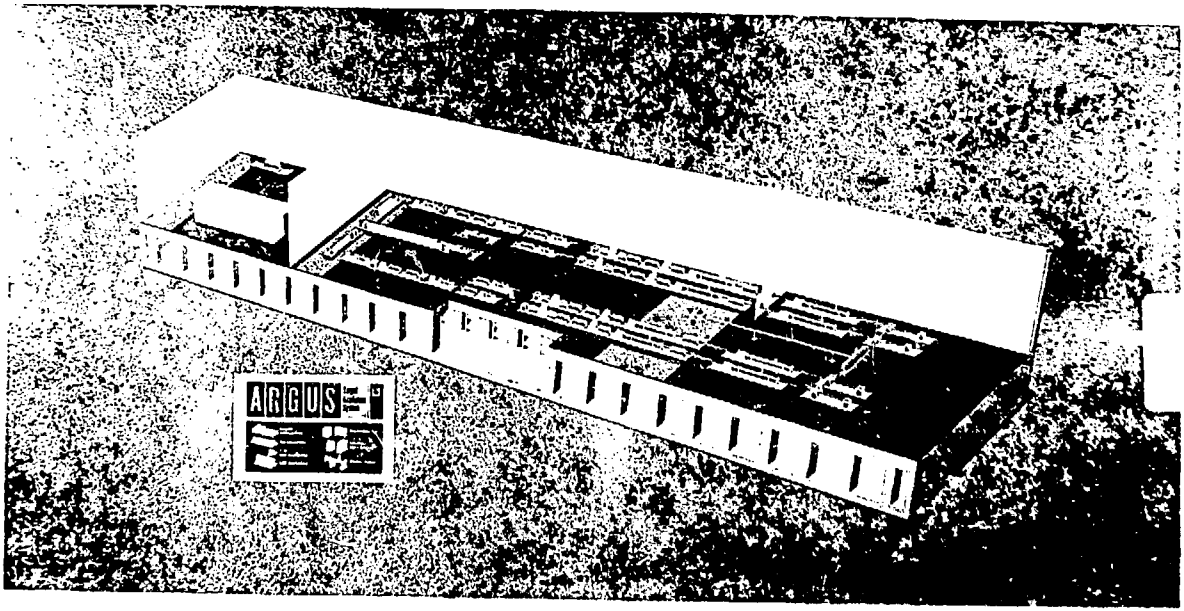
ARGUS

JANUS – TARGET AND BEAM IMAGING OPTICS

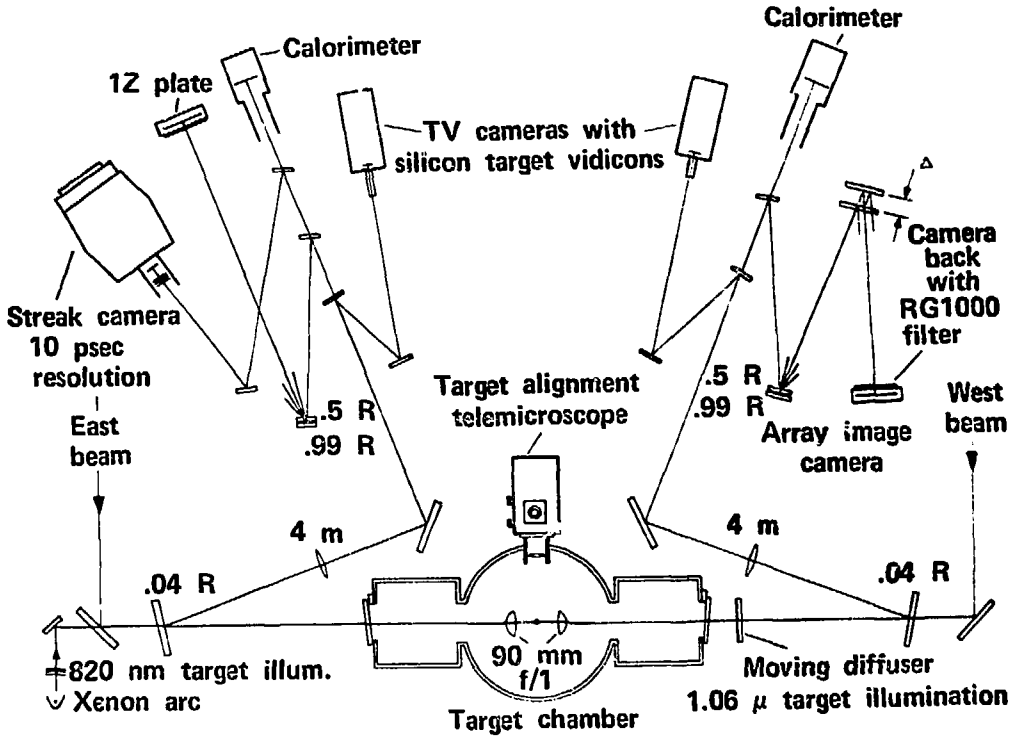

X-RAY STREAK CAMERA

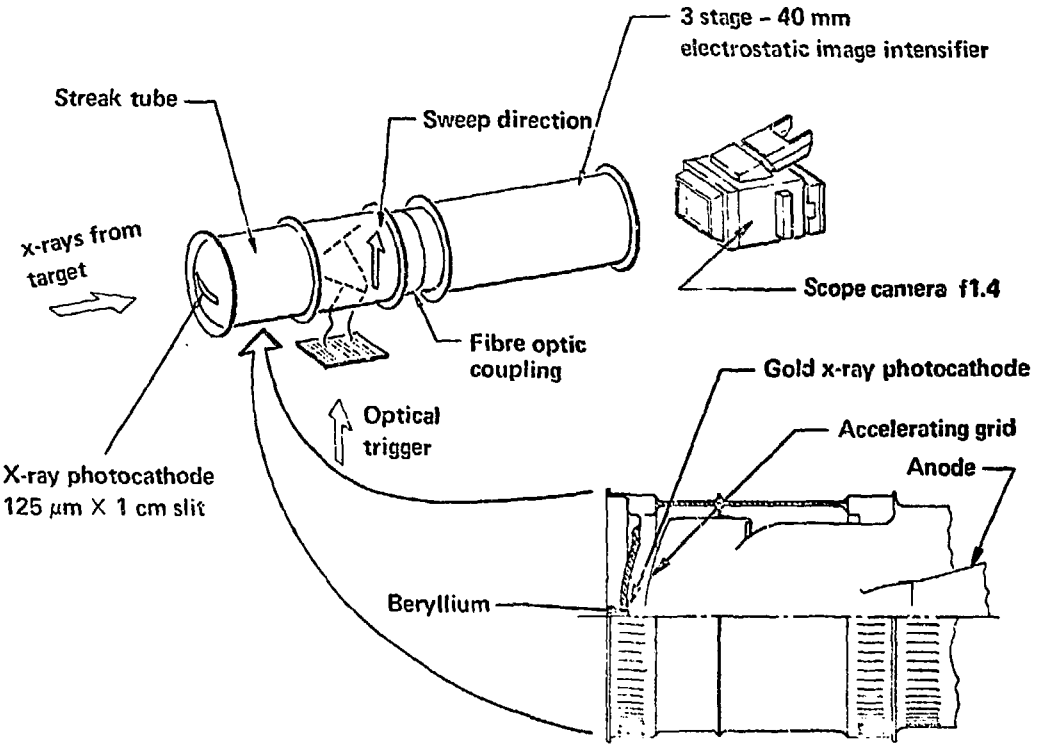

TIME RESOLVED X-RAY EMISSION

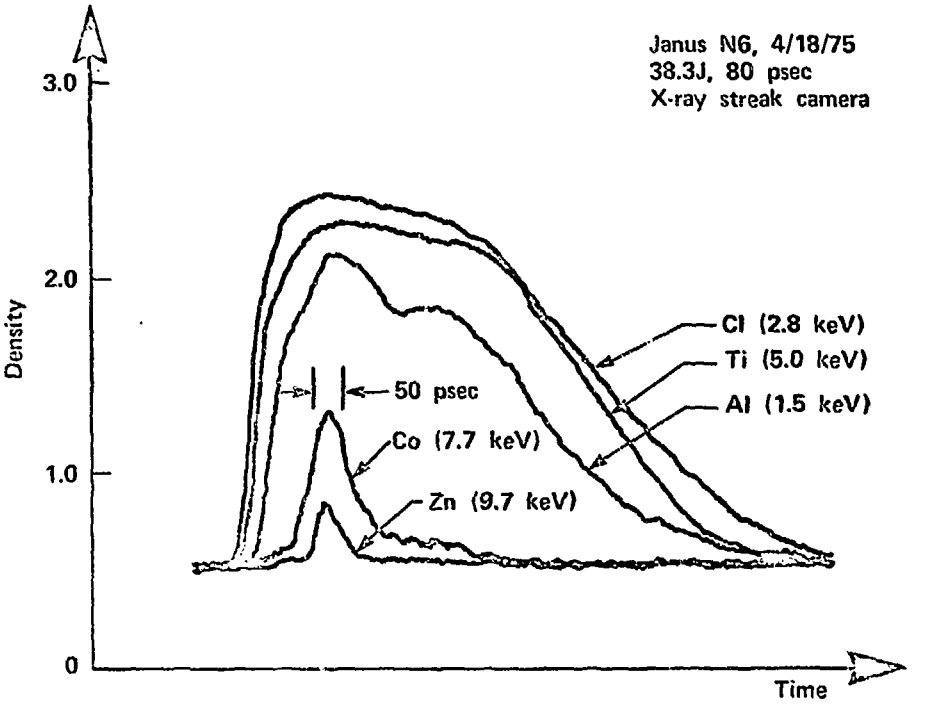

SCHEMATIC OF ENERGY BALANCE DIAGNOSTICS (TOP VIEW)

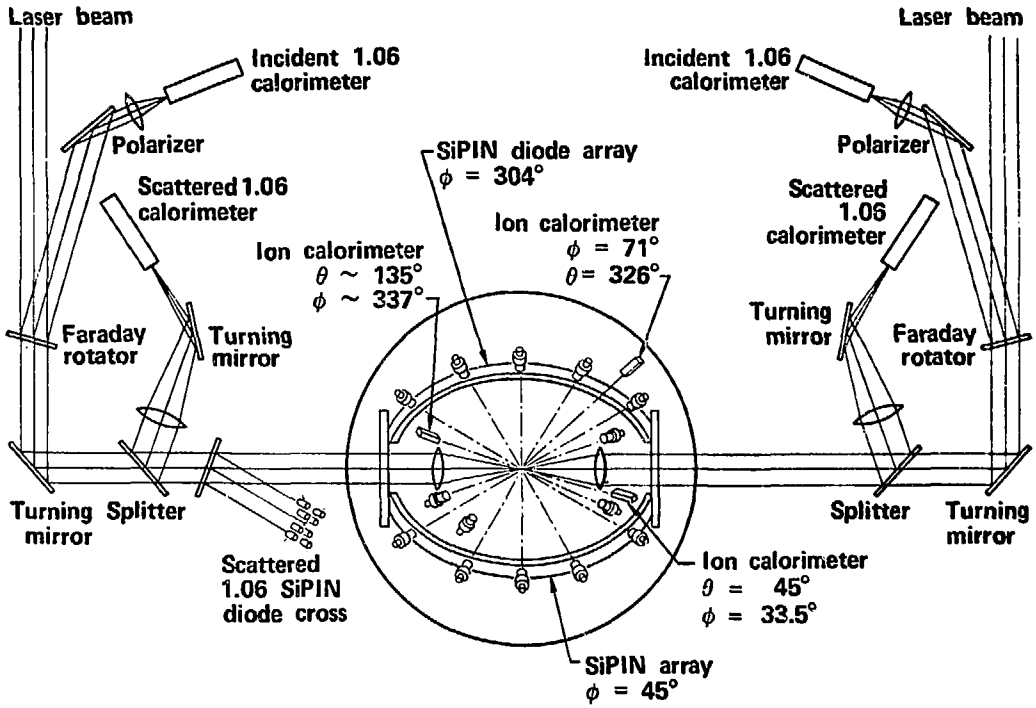

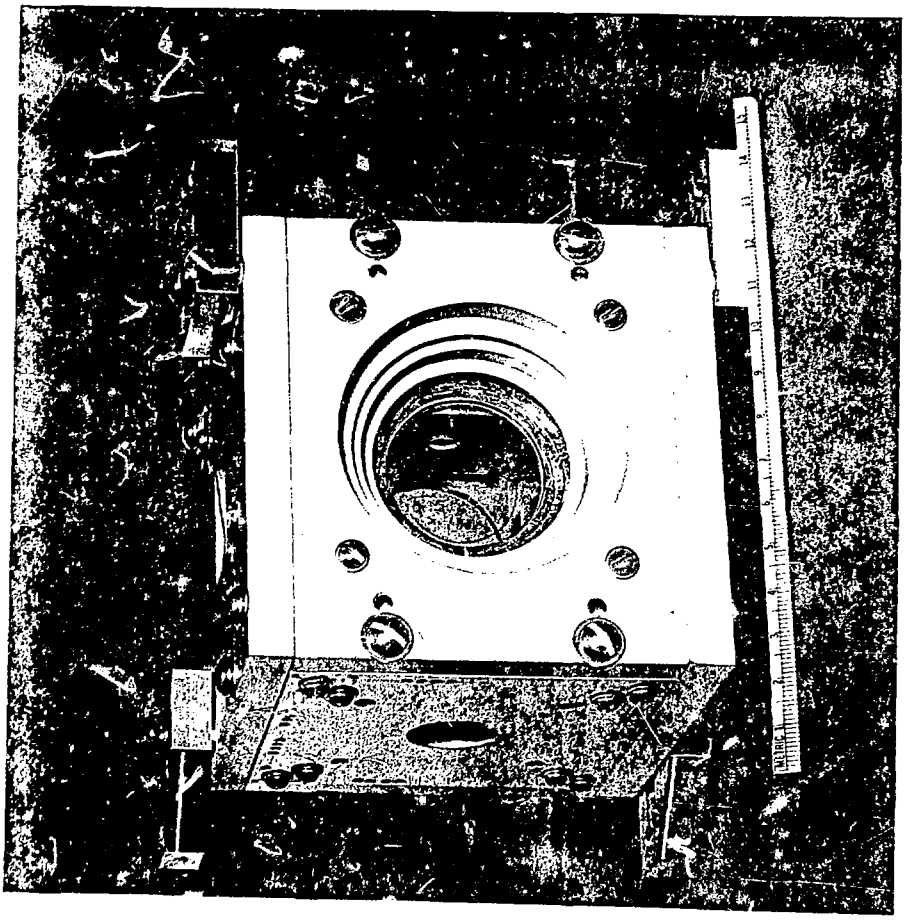

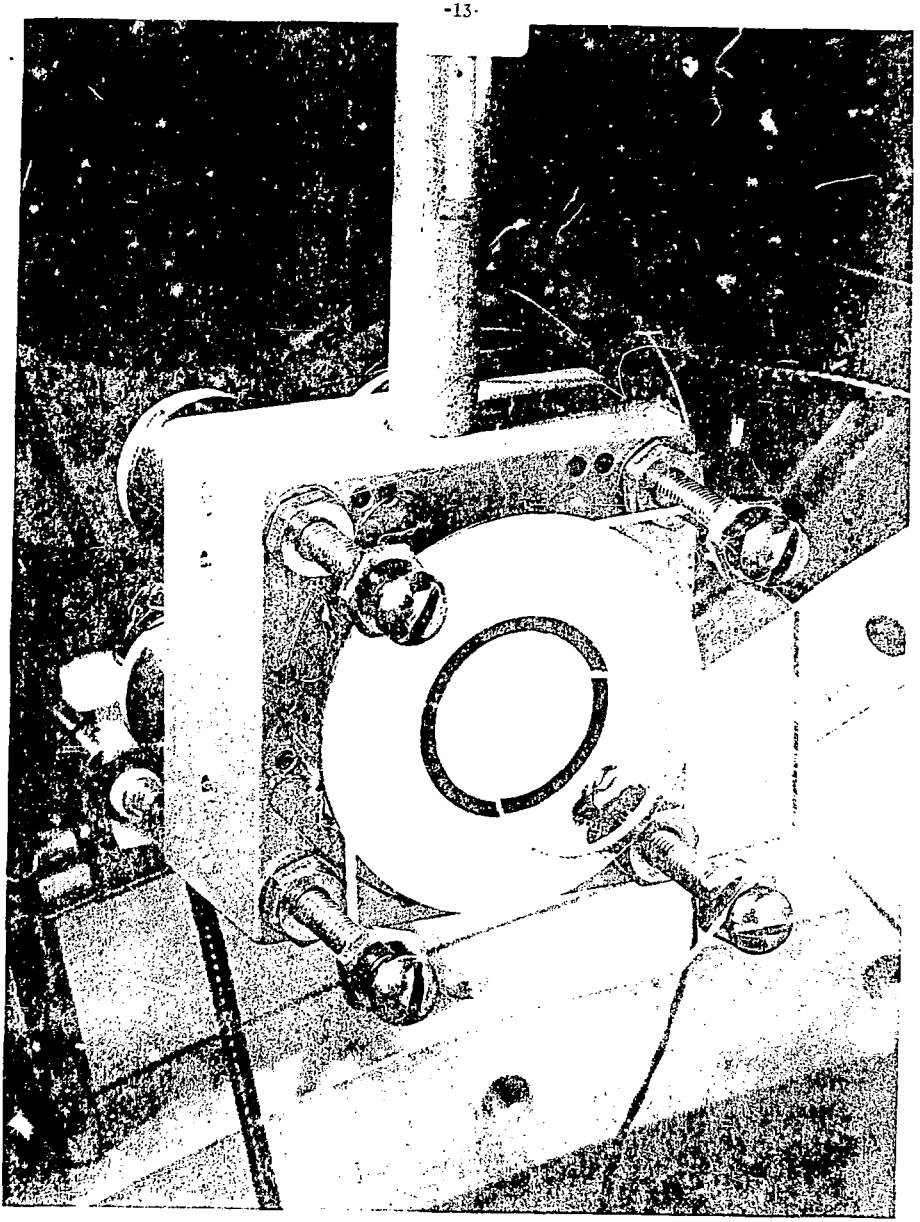

SIMPLE 4-CHANNEL X-RAY MICROSCOPE

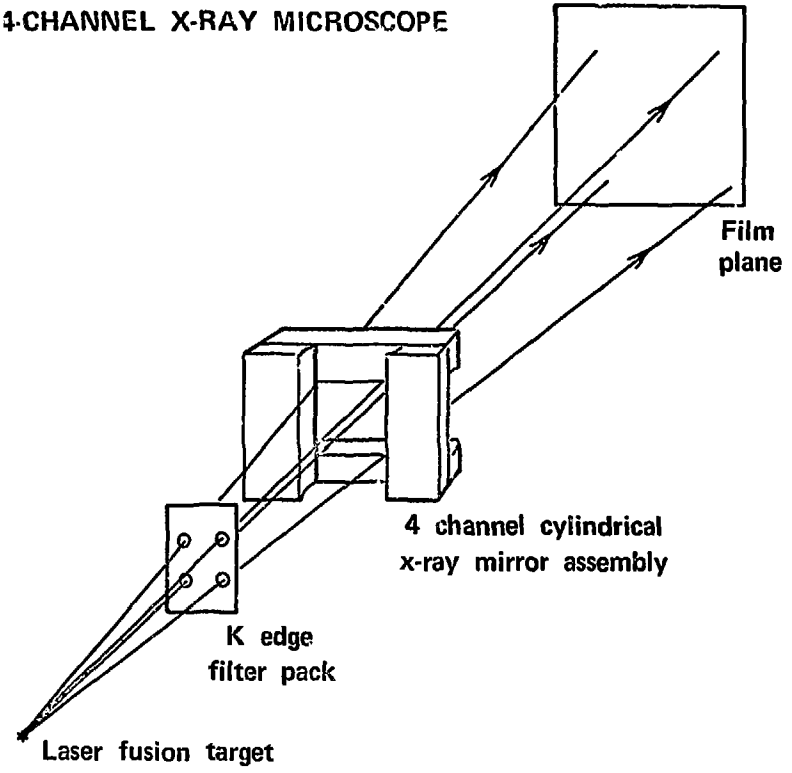

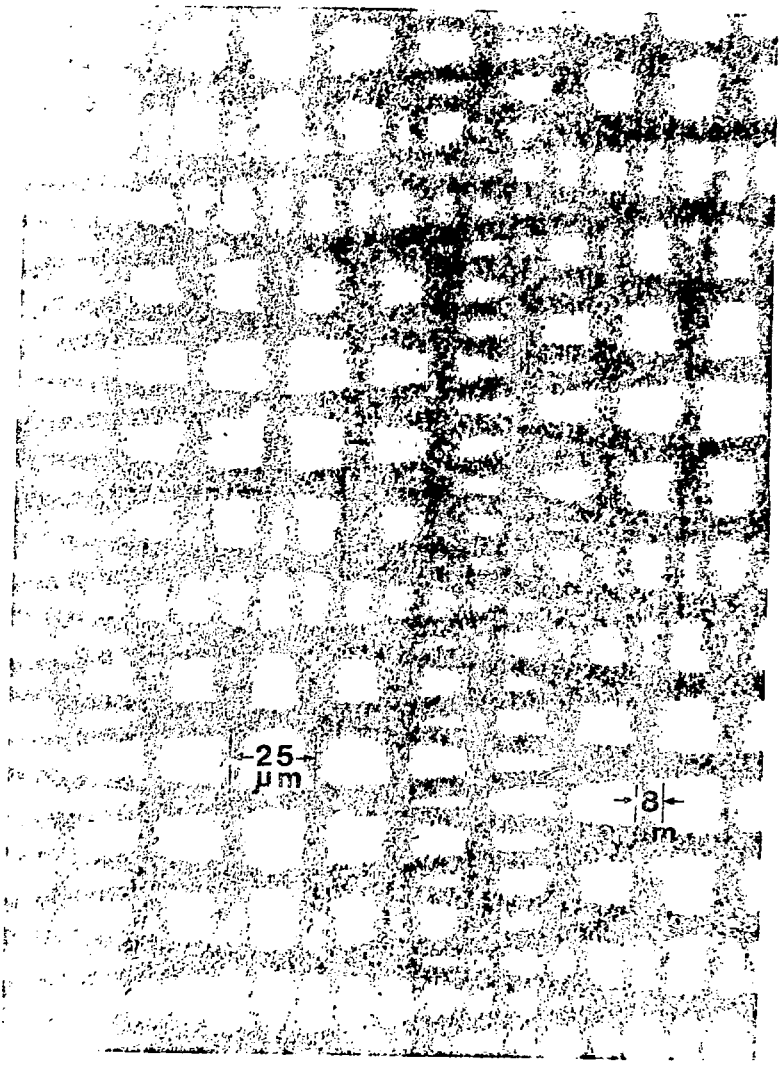

Wire grid resolution

DENSITOMETER TRACES OF WIRE GRID

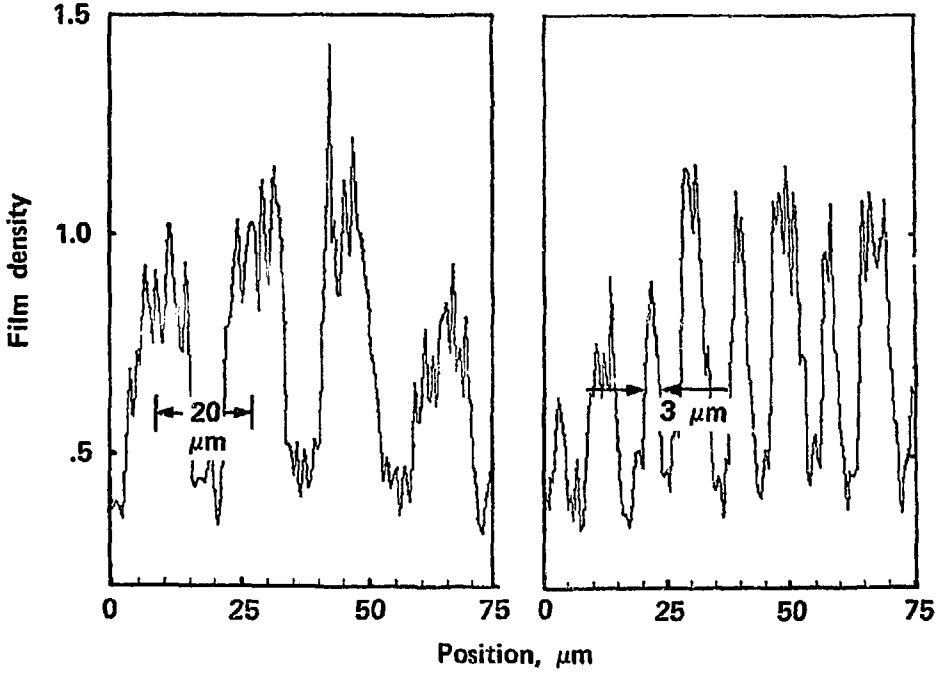

WOLTER TYPE I X-RAY MICROSCOPE SCHEMATIC

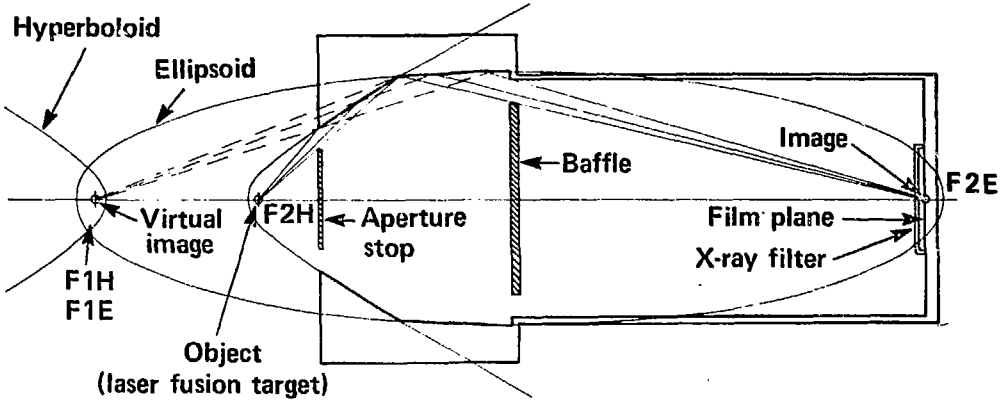

6X WOLTER MICROSCOPE RESOLUTION VS OFF-AXIS OBJECT POSITION

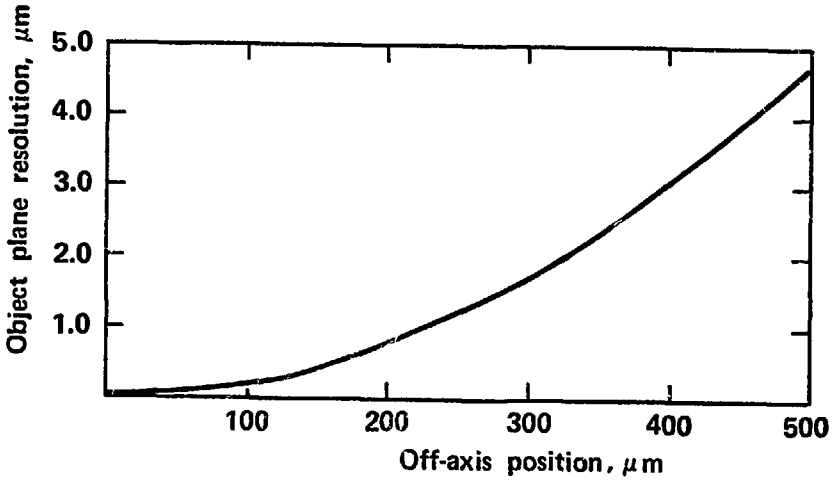

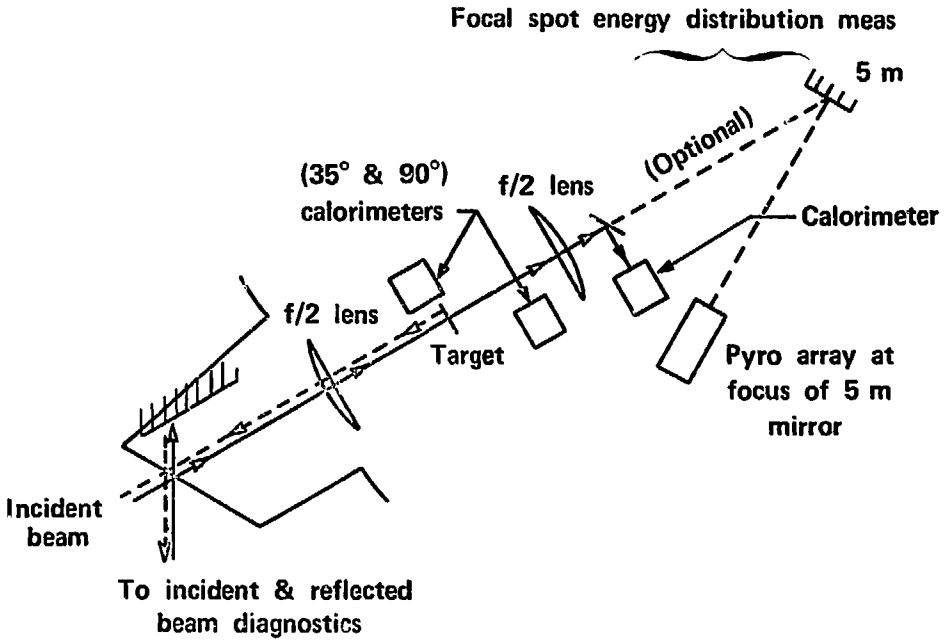
Focal spot energy distribution meas
5 m
(Optional)
(35° & 90°)
calorimeters
f/2 lens
Calorimeter
f/2 lens
Target
Pyro array at
focus of 5 m
mirror
Incident
beam
To incident & reflected
beam diagnostics

CO_2 LASER SYSTEM BEAM UNIFORMITY

Near field at lens:

Pyro-array photograph

ω_1 ~ 1.6 ± 0.1 cm

Burn pattern

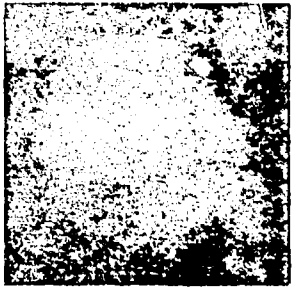

Far field in focus:

Pyro-array photograph

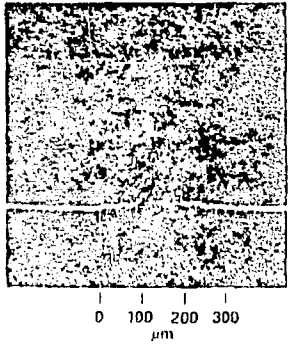

ω_0 ~ 68 ± 5 μm

Burn pattern

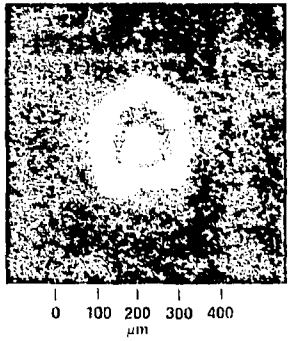

JANUS WITH TWO f/1 LENSES

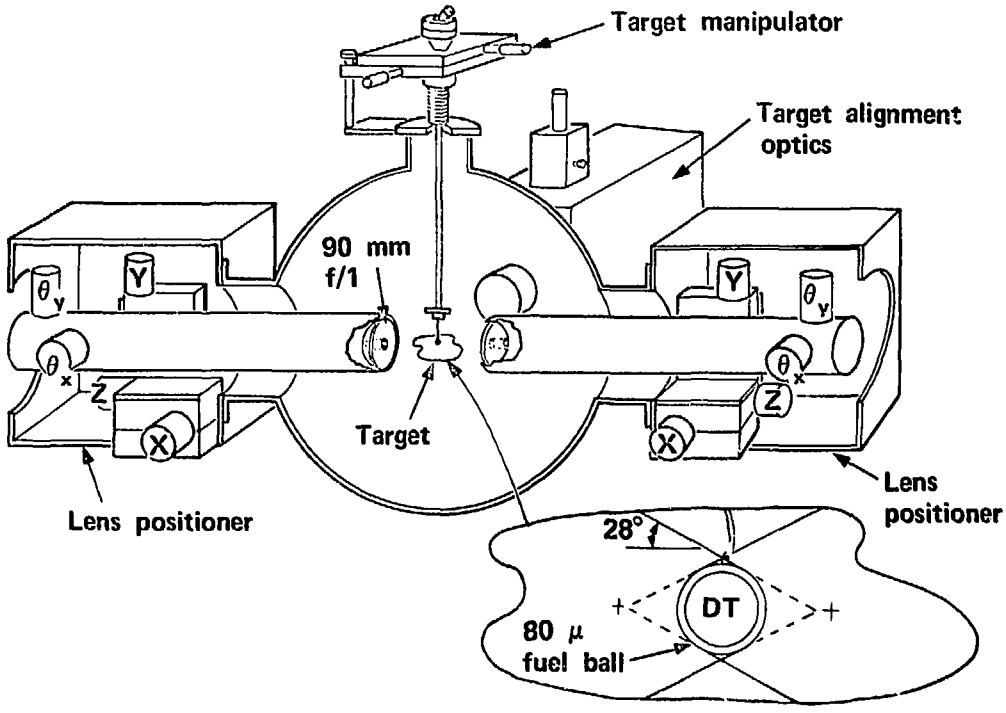

JANUS – FOCAL REGION AT 0.4 TW

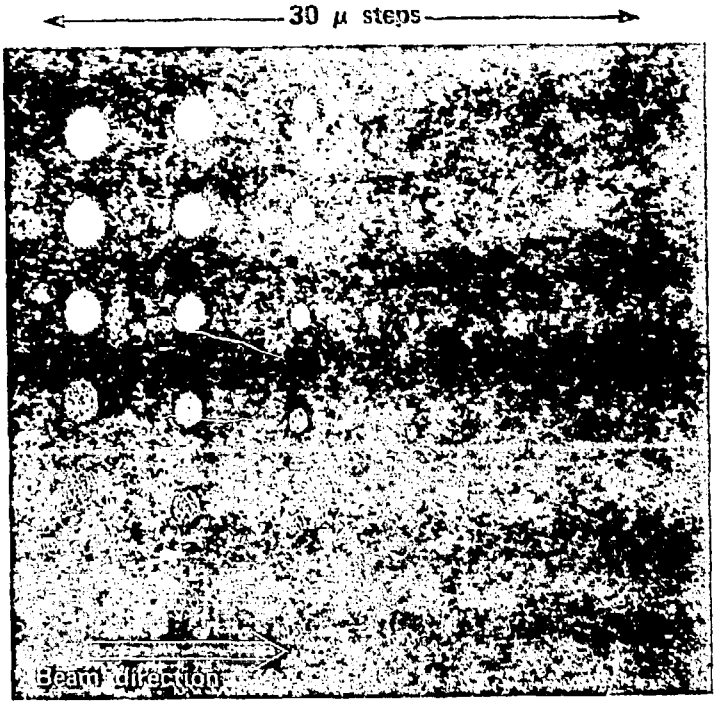

East beam 6/19/75
16.9 J/92 psec = 184 GW each beam

JANUS – ENERGY INCIDENT ON TARGET

Energy contours

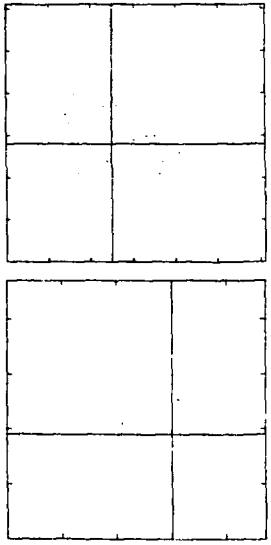

Traces through center

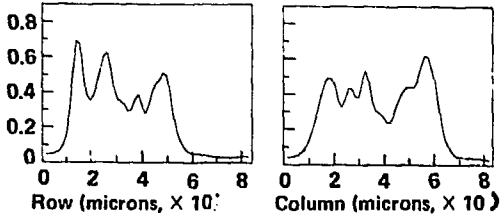

Low Power

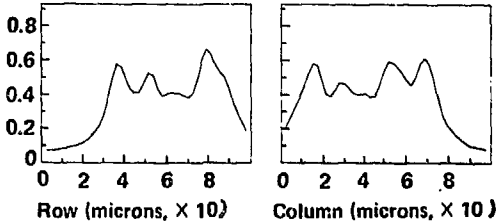

High Power

JANUS SPHERICAL ILLUMINATION SYSTEM

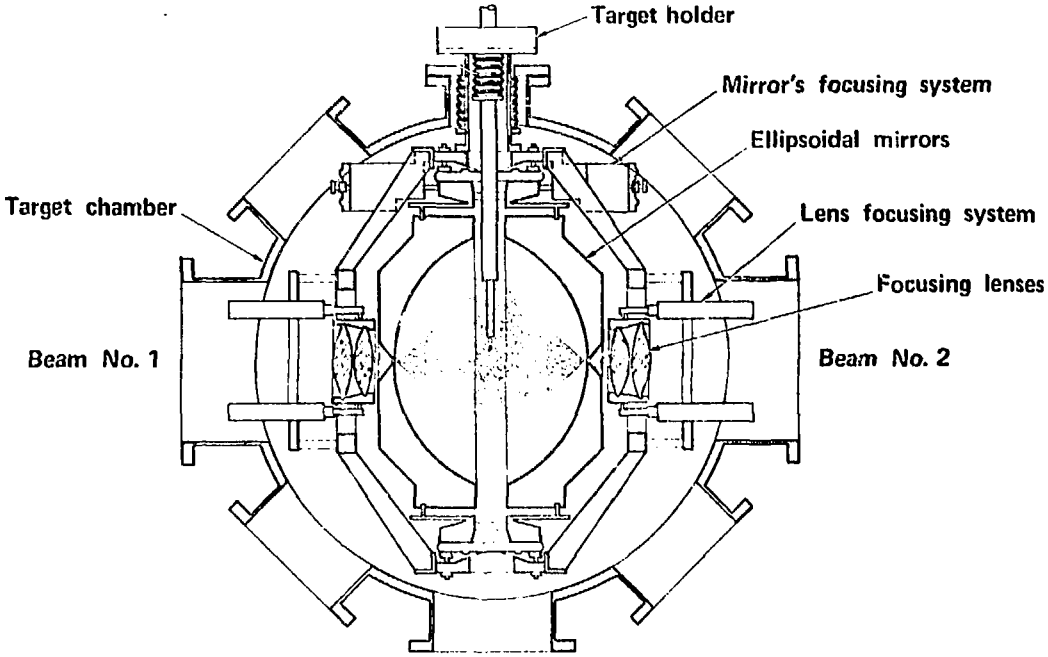

JANUS SPHERICAL ILLUMINATION TARGET INTENSITY DISTRIBUTION

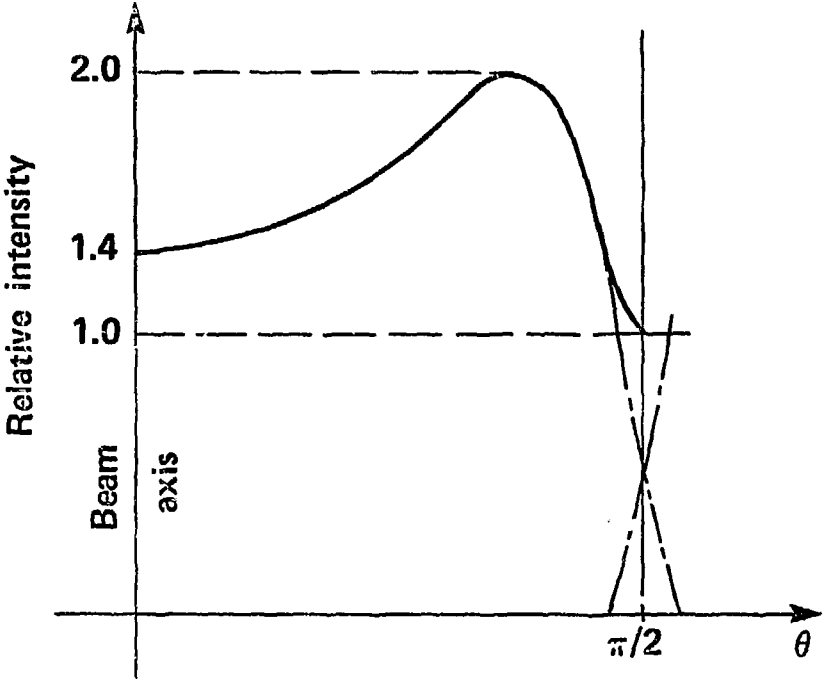

CYCLOPS TARGET CHAMBER

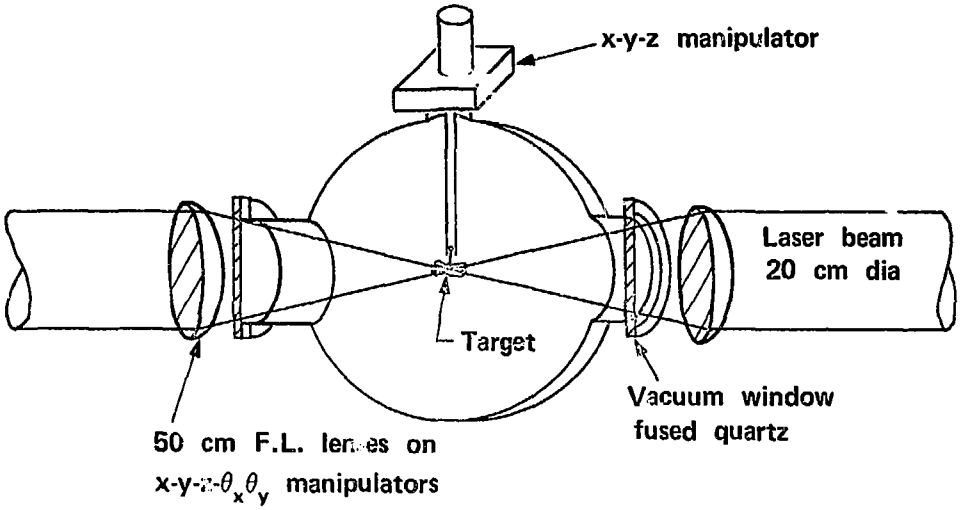

ARGUS SPHERICAL ILLUMINATION SYSTEM

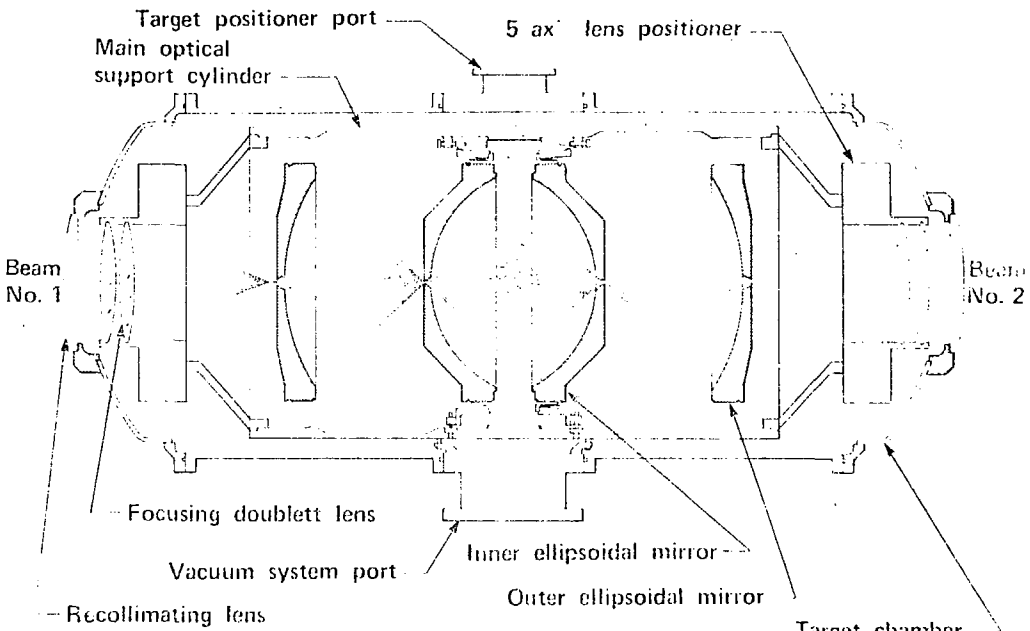

ARGUS SPHERICAL ILLUMINATION TARGET INTENSITY DISTRIBUTION

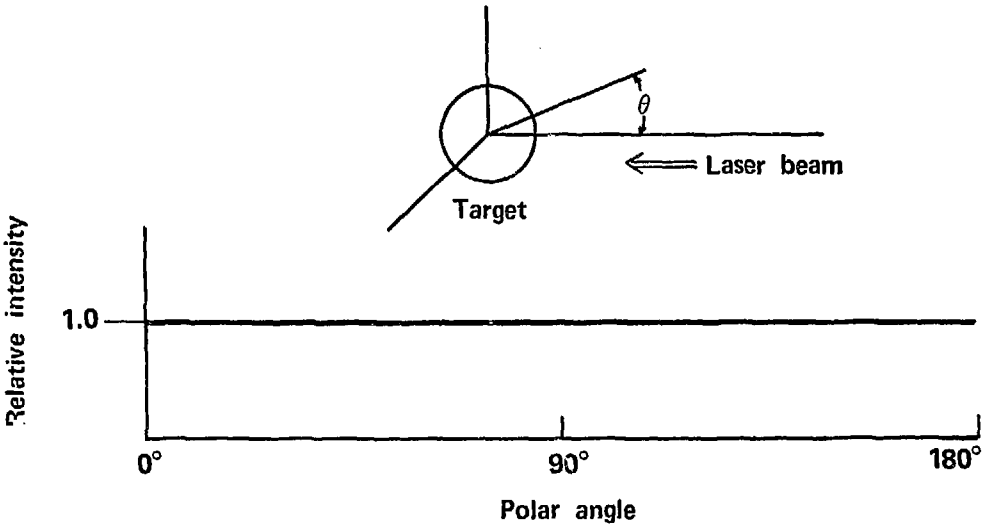

SUMMARY – 10.6 μm LASER/FOIL AND DISK EXPERIMENTS

Shot Number	Target	Focal spot (fwhm)	ϵ_L (J)	τ_L (nsec)	I_L (W/cm^2)	ϵ_R (J)	ϵ_T (J)	v_{FS} (cm/sec)	v_{BS} (cm/sec)	$(E_i/A)^\dagger$ (keV/amu)	T_e* (keV)	αT_e** (keV)	X-ray*** emission region (dia.-μm)
1956	5μm foil	80μm	25.4	1.4	2.4×10^{14}	.12		9.4×10^6			.3-.5	20	
1957	↓	↓	19.4	1.4	1.8×10^{14}	.08		1.3×10^7			↓	70	
1958			20.5	3.2	8.5×10^{13}	.10		3.7×10^6		(3.6)		38	
								2.2×10^7					
1997			15.0	3.4	5.8×10^{13}	.07	$< .07$	4.8×10^6		.03 (2.3)		39	
								1.1×10^7					
1999	↓		14.1	4.1	4.5×10^{13}	.06	$< .07$	4.6×10^6		.06 (7.6)		45	
								1.4×10^7					
1951	10μm foil		19.8		7.1×10^{13}	.14						19	
1952	↓		19.4	1.4	1.8×10^{14}	.12	1.5			.57 (1.0)		21	
1954			20.9	1.4	2.0×10^{14}	.08	.58			.41 (1.3)		19	
1983	5μm foil		22.7	3.2	9.4×10^{13}	.13	.15					47	200
1989	↓		14.0	2.1	8.8×10^{13}		$< .07$					47	170
1991			11.5	2.1	7.2×10^{13}	.06	.22			.08 (1.5)		55	215
1967	5μm disk		18.1	4.1	5.7×10^{13}	.02	5.3	5.4×10^6	3.9×10^6	3.4		142	
1979	↓		18.8	3.7	6.7×10^{13}		.22	7.7×10^6		8.8		48	240/900
1980			17.0	2.6	8.4×10^{13}	.02	.73			12.0		48	215/850
1981			23.1	2.6	1.1×10^{14}	.01	.40	4.5×10^6	8.6×10^5			49	240/1020
1982			20.2	3.6	7.2×10^{13}	.02	.31	4.0×10^6	5.0×10^6			6.7	195/1075
								1.2×10^7					
1990			15.0	2.1	9.5×10^{13}	.05	.39	4.6×10^6	3.6×10^6	8.8		32	170/1130
2003			14.1	2.1	8.9×10^{13}	.02	.44	1.0×10^7		3.4 (10.0)		24	215/745
1977	↓	↓	18.5	1.4	1.7×10^{14}	.02		1.6×10^7	3.7×10^6		↓	1141	215/850

† E_i/A at the peaks of the emitted ion energy distribution

* Estimate based on x-ray photographs and emission (≥ 1 keV) measurements

** Based on high energy tail of emitted electron distribution

*** Notation for 5μm disk data presents the horizontal extent and vertical extent of the x-ray emitting regions associated with emission from the disk and stalk regions of the target.

SPATIAL DISTRIBUTION OF X-RAY EMISSION (10.6 μm LASER)

25 μm unfiltered pinhole

$I_p \simeq 9.4 \times 10^{13}$ W/cm^2
5 μm polyethylene foil

$I_p \simeq 6.7 \times 10^{13}$ W/cm^2
5 μm $\times$ 170 μm dia parylene disk

Front surface

Back surface

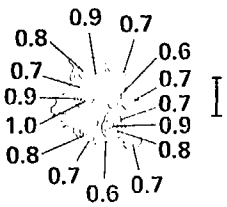

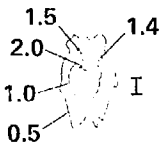

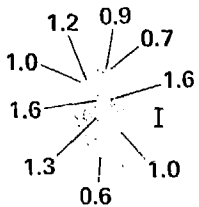

I denotes 100 μm

streak time 2.47 nsec
field of view 650 μm

5 μm polyethylene foil
$I_p \simeq 4.8 \times 10^{13}$ W/cm^2

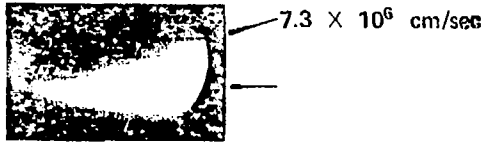

5 μm X 150 μm dia. parylene disk
$I_p \simeq 5.7 \times 10^{13}$ W/cm^2

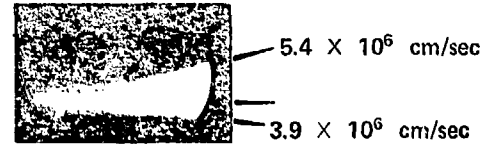

$I_p \simeq 8.5 \times 10^{13}$ W/cm^2

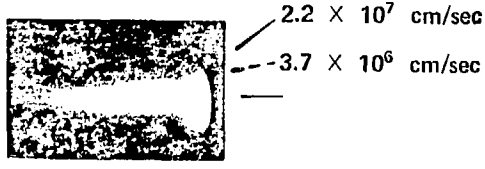

$I_p \simeq 9.5 \times 10^{13}$ W/cm^2

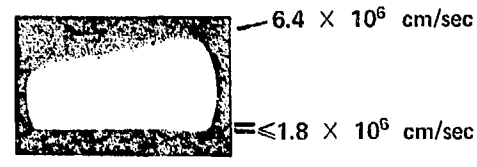

SUMMARY – 1.06 μm LASER/DISK EXPERIMENTS

Shot Number	Target	Focal spot (diam.)	ϵ_L (J)	τ_L (psec)	I_L (W/cm^2)	ϵ_R (J)	ϵ_T (J)	$\epsilon_{abs}/\epsilon_L$ (%)	$(E_i/A)^\dagger$ (keV/amu)	T_e^* (keV)	αT_e^* (keV)	αT_e^{**} (keV)
750225-4	10μm disk	90μm	11.3	102	1.7×10^{15}	3.2	1.38		.58		10	
750225-9		90	12.2	105	1.8×10^{15}	1.5	.81		.63		10	
750301-9		100	10.2	108	1.2×10^{16}	1.1	.48		.63	.53	9.4	
750301-12		45	13.9	94	9.2×10^{15}		.42		.07	.60	20	
750612-8		90	9.7	82	1.8×10^{16}	3.4	.63	16°	.47 (49.5)	.89	19	
750627-13		90	6.2	62	1.6×10^{15}	2.3	.41	15°	.48 (65)	.57	12	25
750627-15		30	6.8	63	1.5×10^{16}	2.2	.36	26°	.60 (94)	.61	21	40
750627-16		30	6.5	72	1.3×10^{16}	2.0	.36	19°	.45 (94)	.68	21	40
750724-7		90	9.8	81	1.9×10^{15}	3.4	.19	30 ± 6°°				
750729-10		30	10.9	67	2.3×10^{16}	2.2	.87	35 ± 5°°				
750729-11		90	5.9	62	1.5×10^{15}	2.0	.14	31 ± 6°°				

° based on photodiode array
°° based on enclosing calorimeter
† E_i/A at the peaks of the emitted ion energy distribution
* Based on x-ray emission spectrum (~ 1 keV – 90 keV)
** Based on high energy electron emission spectrum (30 – 199 keV)

AVERAGED ANGULAR DISTRIBUTION OF SCATTERED 1.06 μm RADIATION/DISK TARGET

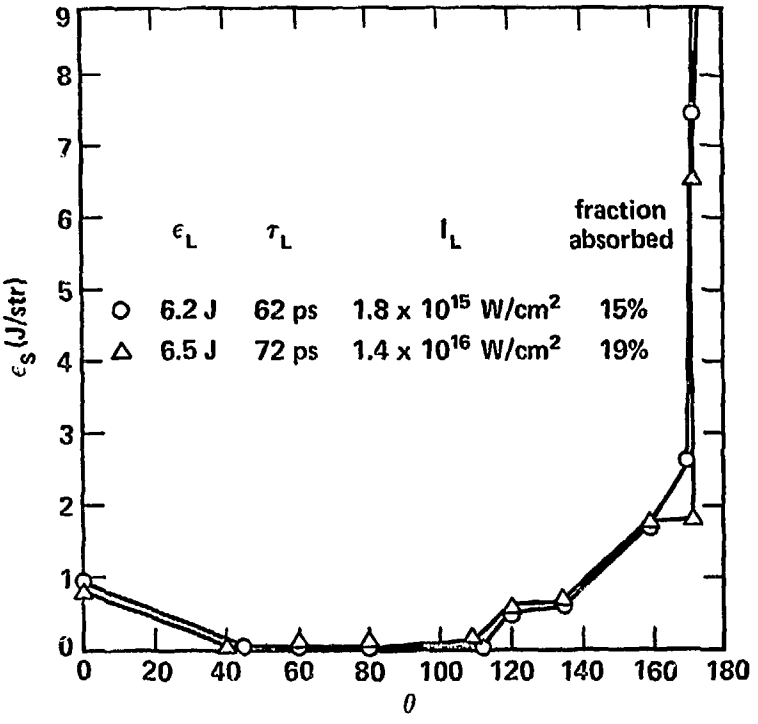

X-RAY SPECTRA – 1.06 μm LASER/DISK TARGET

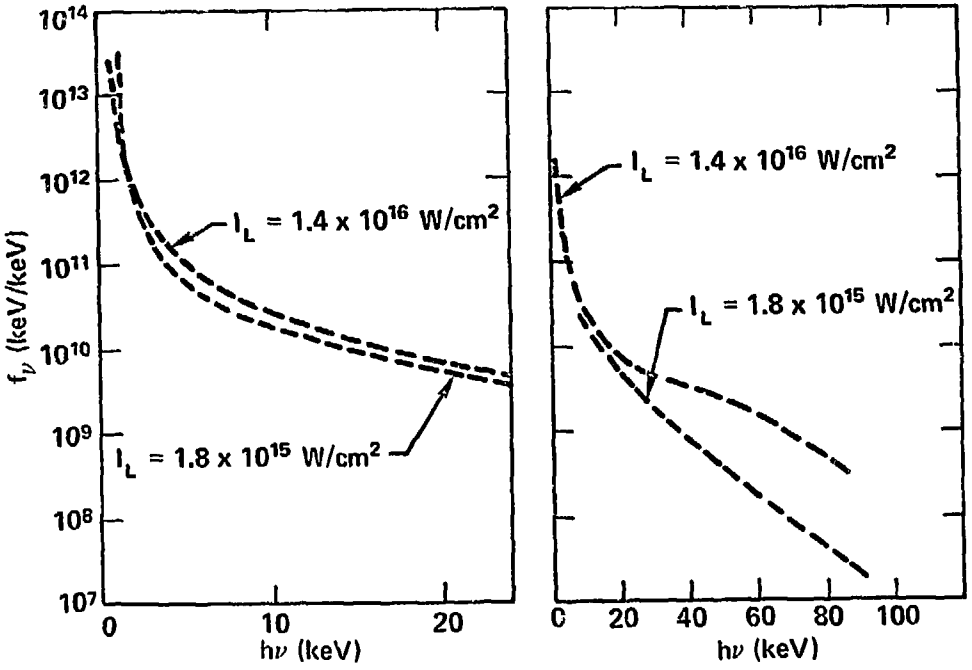

ELECTRON SPECTRA — 1.06 μm LASER/DISK TARGET

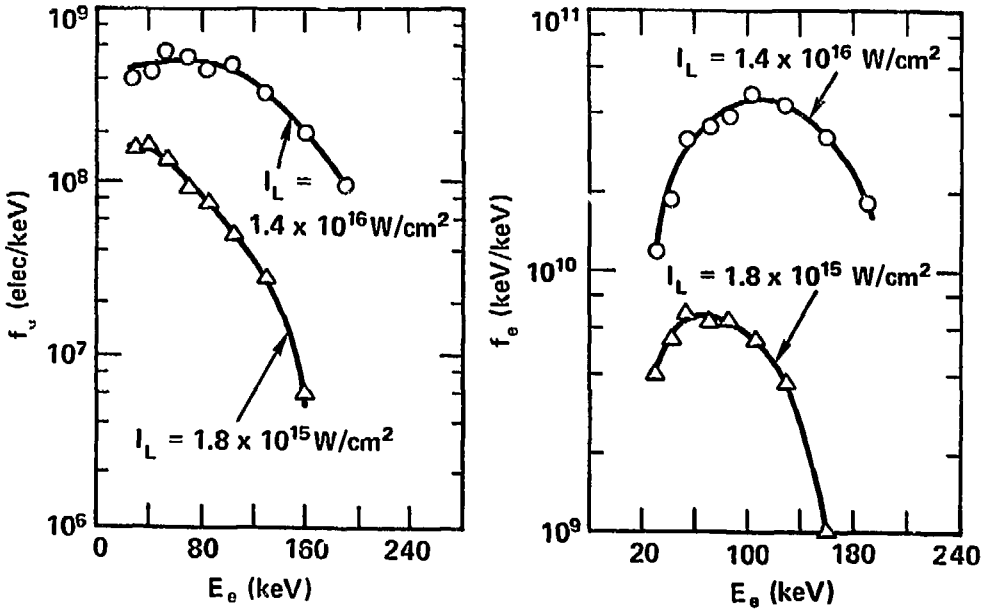

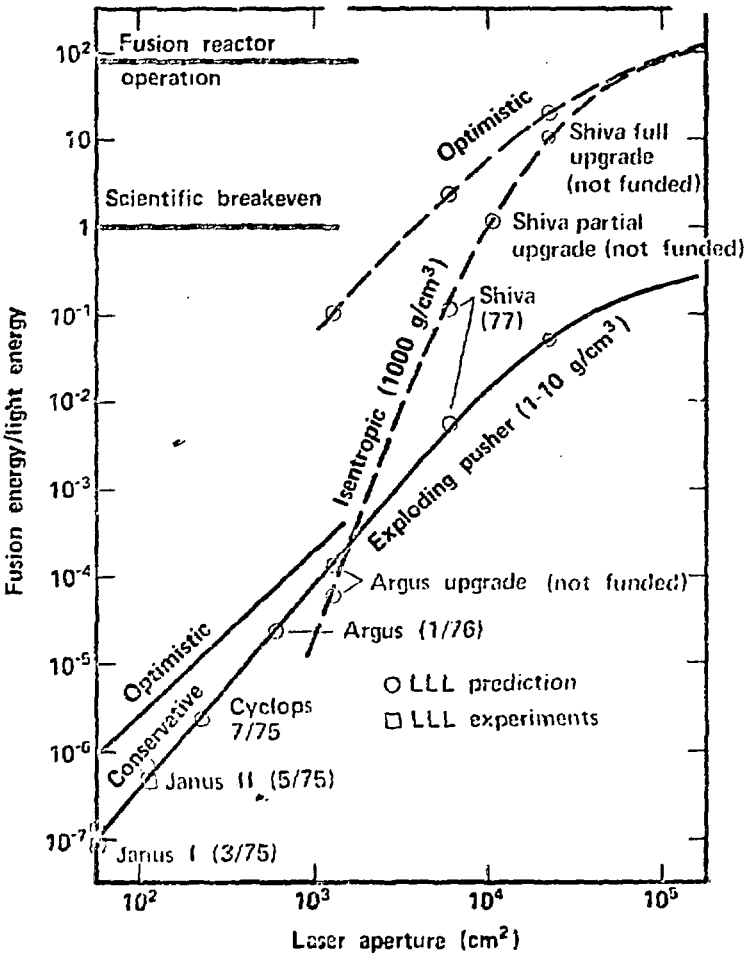
Fusion reactor operation
Scientific breakeven
Optimistic
Shiva full upgrade (not funded)
Shiva partial upgrade (not funded)
Shiva (77)
Isentropic (1000 g/cm³)
Exploding pusher (1-10 g/cm³)
Argus upgrade (not funded)
Argus (1/76)
Optimistic
Conservative
Cyclops 7/75
Janus II (5/75)
Janus I (3/75)
O LLL prediction
□ LLL experiments
Fusion energy/light energy
Laser aperture (cm²)

SPHERE AND PLANE TARGET

(a)

O.D. = 115

(b)

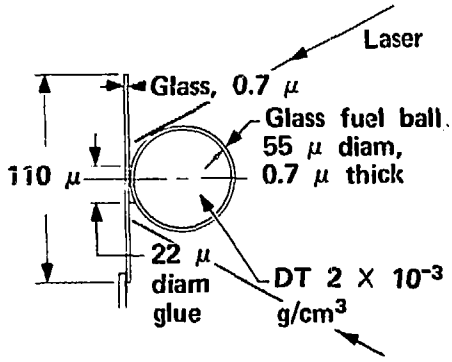

Laser energy to target	15 joules
Laser pulse duration	90 psec (Gaussian)
Energy absorbed	3.6 joules
Neutron yield	1.1×10^4

Compression (calculated)	50
Ion temperature	700 eV
Electron temperature	350 eV

X-RAY SPECTRUM OF BALL-ON-DISK TARGET (J11, 2/26/75)

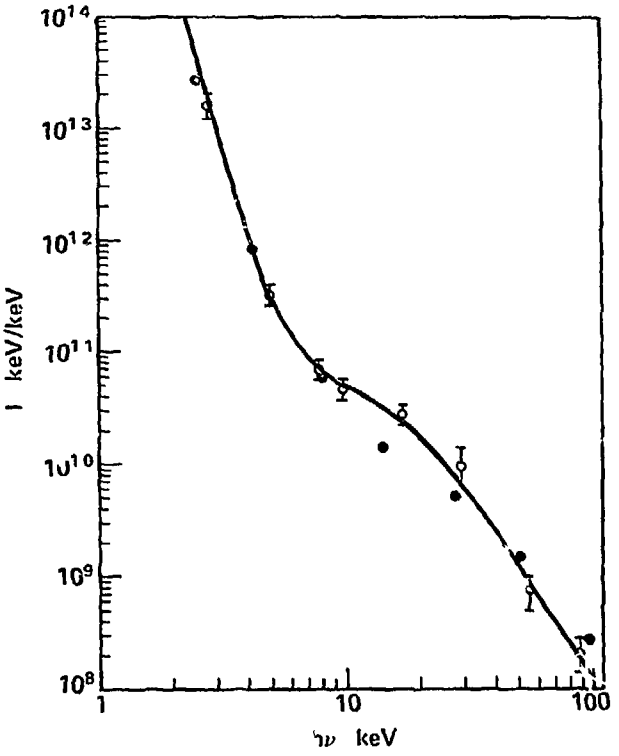

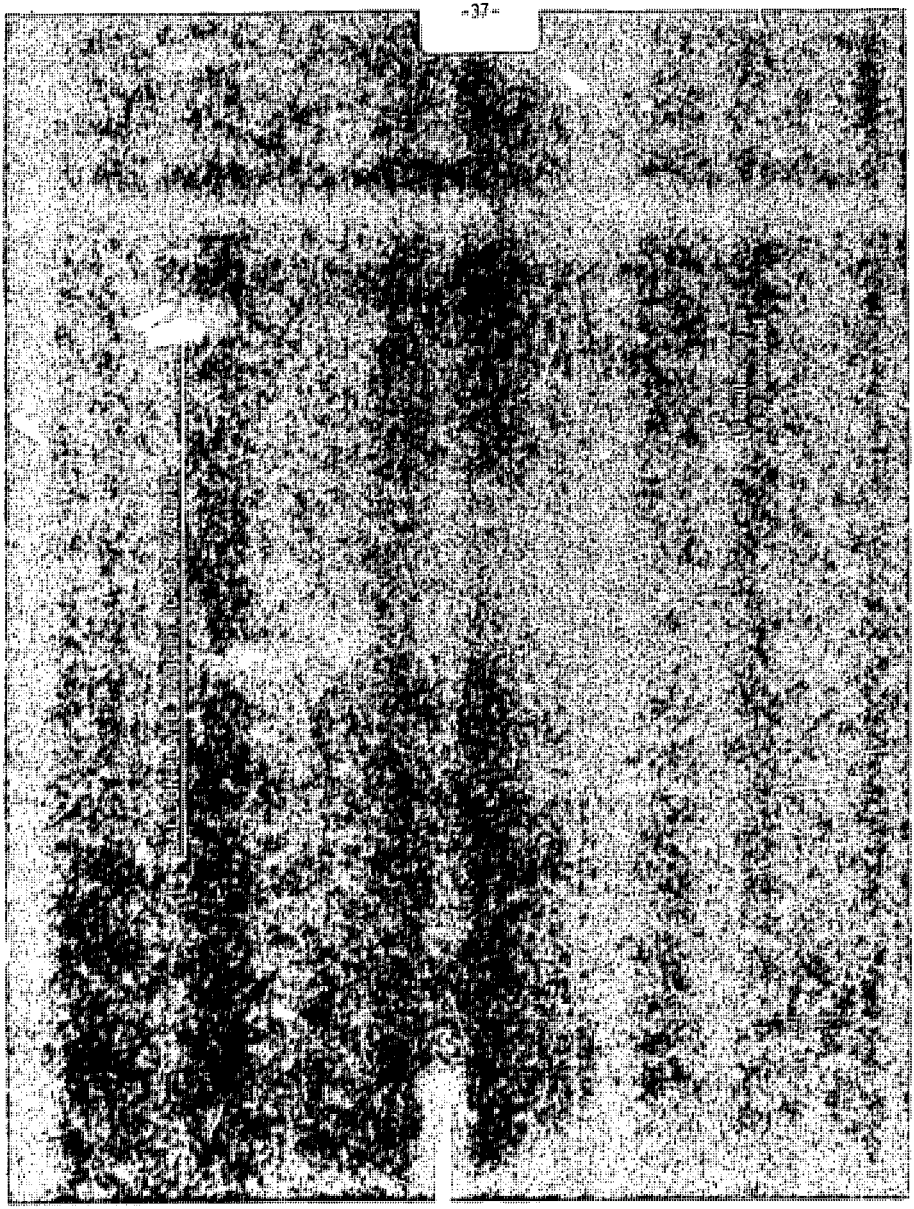

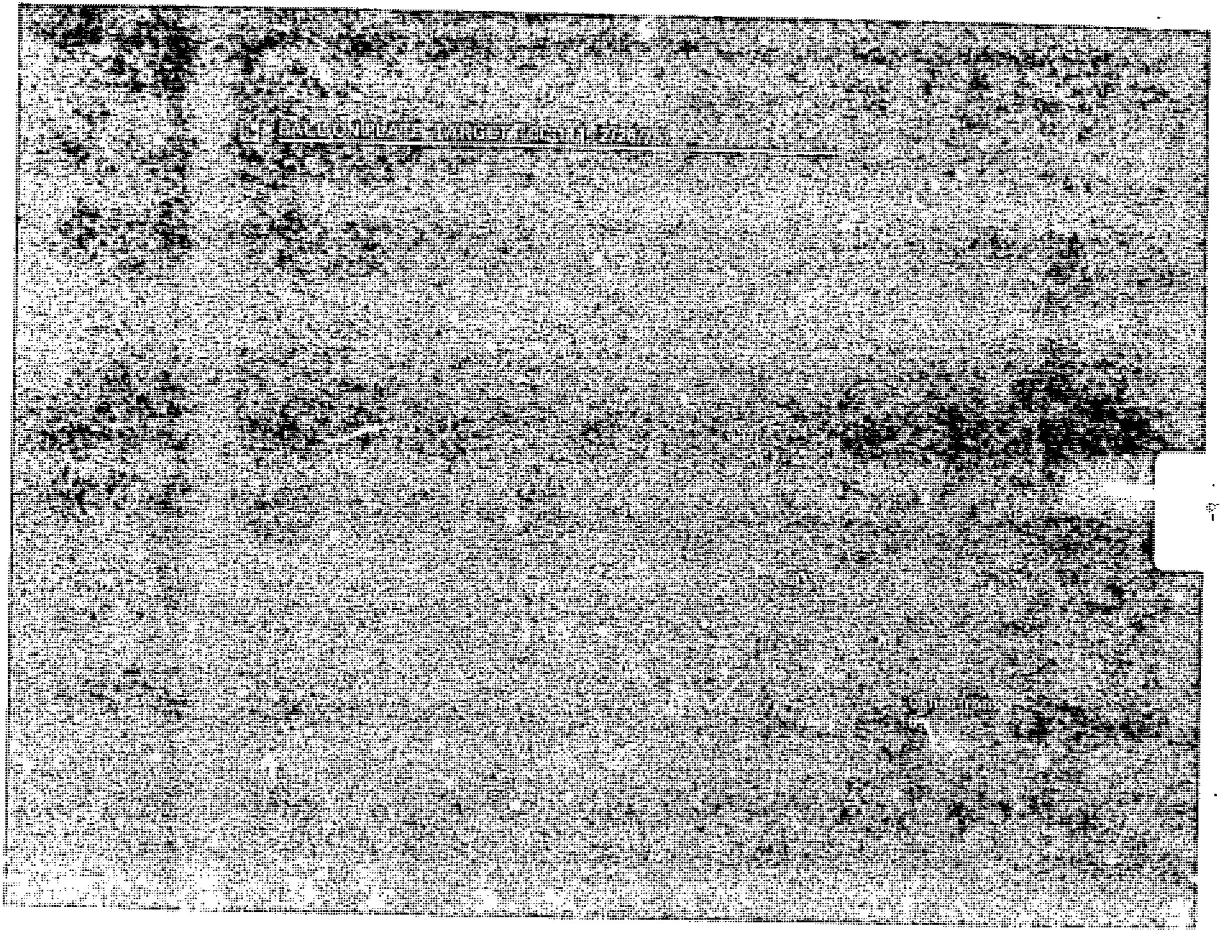

BAIL-IN-PLATE TARGET (SC-4)

Side view

Front view

BALL-IN-PLATE TARGET SC-4 4-17-75

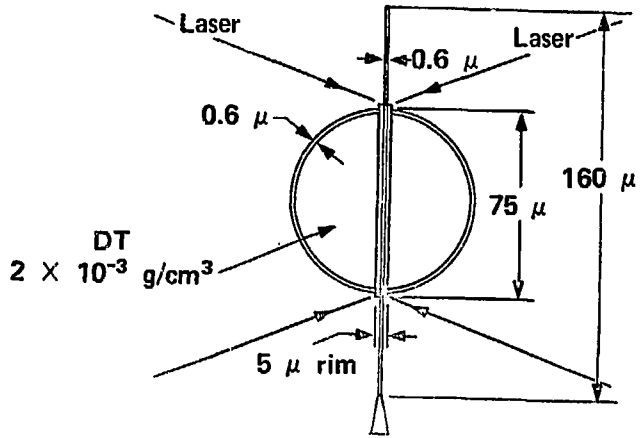

Laser energy
East 14 J
West 14.6 J

Laser pulse
(~Gaussian) 70 ps

Absorbed energy 9 J

Calculated parameters
T_{ion} ~ 1.5 keV
T_{elec} ~ 700 eV
Compression 80

X-RAY SPECTRUM OF BALL-IN-PLATE TARGET (SC-1, 4/24/75-3)

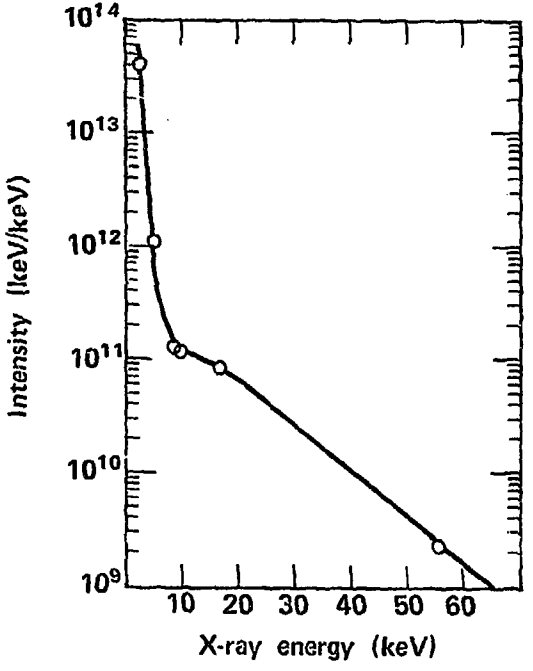

800 eV channel

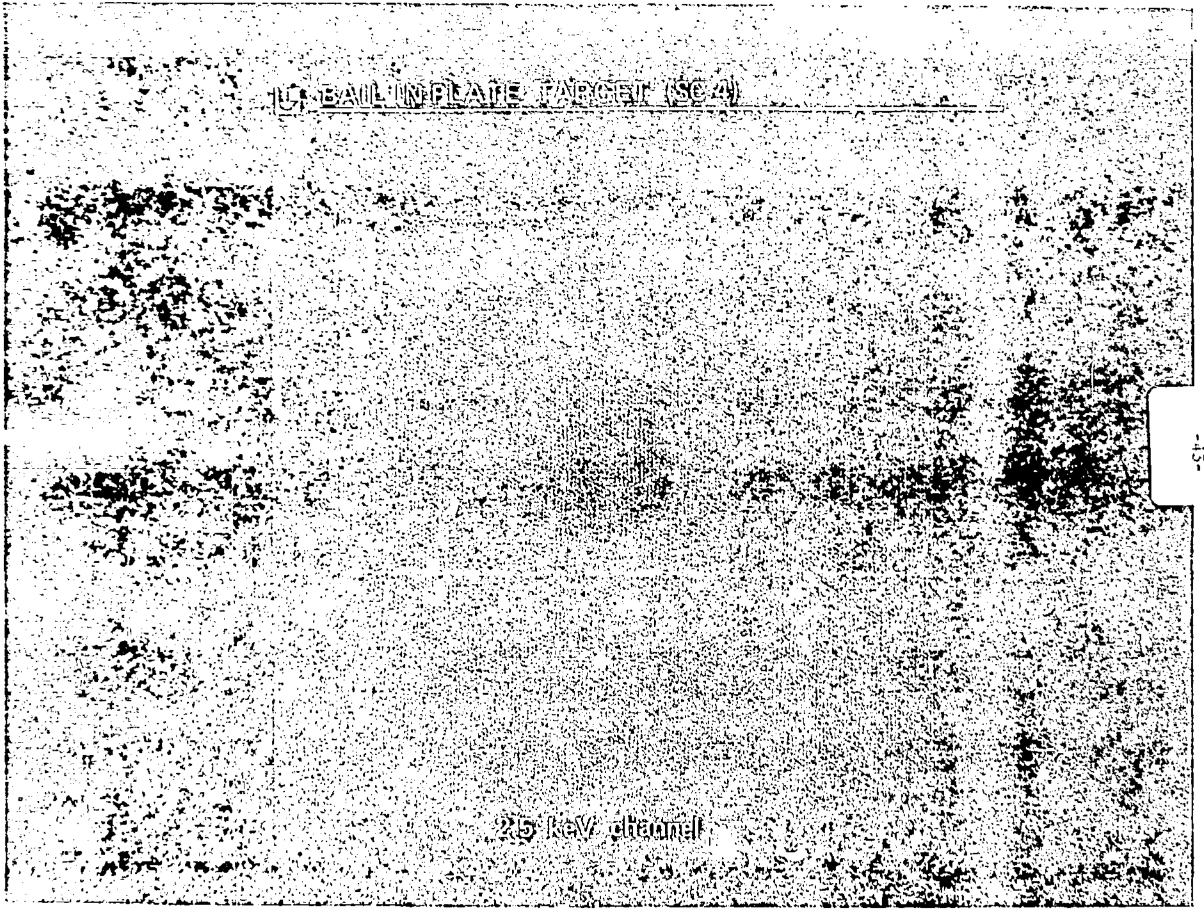
C. BALL IN PLATE TARGET (SC 4)
2.5 keV channel

SUMMARY OF BALL-ON-STALK EXPERIMENTS

Shot-ID	E_W (Joules)	E_E (Joules)	E_A (Joules)	FWHM (psec)	D (μ)	W (μ)	M (ng)	Fill mg/cm^3	$\Delta\tau$ (psec)	N	Ti (keV)	Te (keV)	αY (keV)
75062405	13.8	14.5	7.4	73	82	0.64	34	2	0	2.0×10^6	1.8-3.6*	0.75	9.9
75062505	14.6	16.5	8.4	75	83	0.94	51	2	42	2.5×10^5	--	0.74	10.6
75062502	13.8	15.3	8.7	69	84	0.75	41	2	84	7.5×10^4	–	0.72	11.1
75062506	0	14.9	4.0	75	88	0.48	29	2	00	2.5×10^4	–	0.83	11.9
75062504	0	13.4	3.5	63	86	1.02	59	5	00	1.6×10^4	–	0.80	11.3
75062404	15.3	15.1	7.3	77	81	0.65	34	0	0	0	–	0.78	9.6
75060708	14.7	12.9	6.7	73	85	0.60	34	0.5	0	5.8×10^5	–	0.81	9.5
75060402	14.5	13.8	8.3	70	87	0.70	41	3	0	4.6×10^6	5.8*	0.71	10.6
75062406	14.0	14.8	8.0	72	86	0.99	57	5	0	1.8×10^6	2.4	0.72	11.1
75060704	19.0	16.6	12.0	73	84	0.97	54	7	0	5.7×10^5	–	0.78	11.8
75060709	18.4	16.9	9.2	74	39	0.62	7.3	2	0	2.4×10^5	–	0.95	12.4
75060711	15.5	14.5	8.8	71	64	0.60	19	2	0	2.8×10^5	–	0.96	12.0
75050603	17.1	16.7	10.1	76	107	0.60	53	2	0	7.2×10^3	–	0.80	11.4

*Double peaked α-particle time-of-flight signal

Note: Ti from the α-particle FWHM is not corrected for broadening caused by Doppler and straggling effects in the plasma.

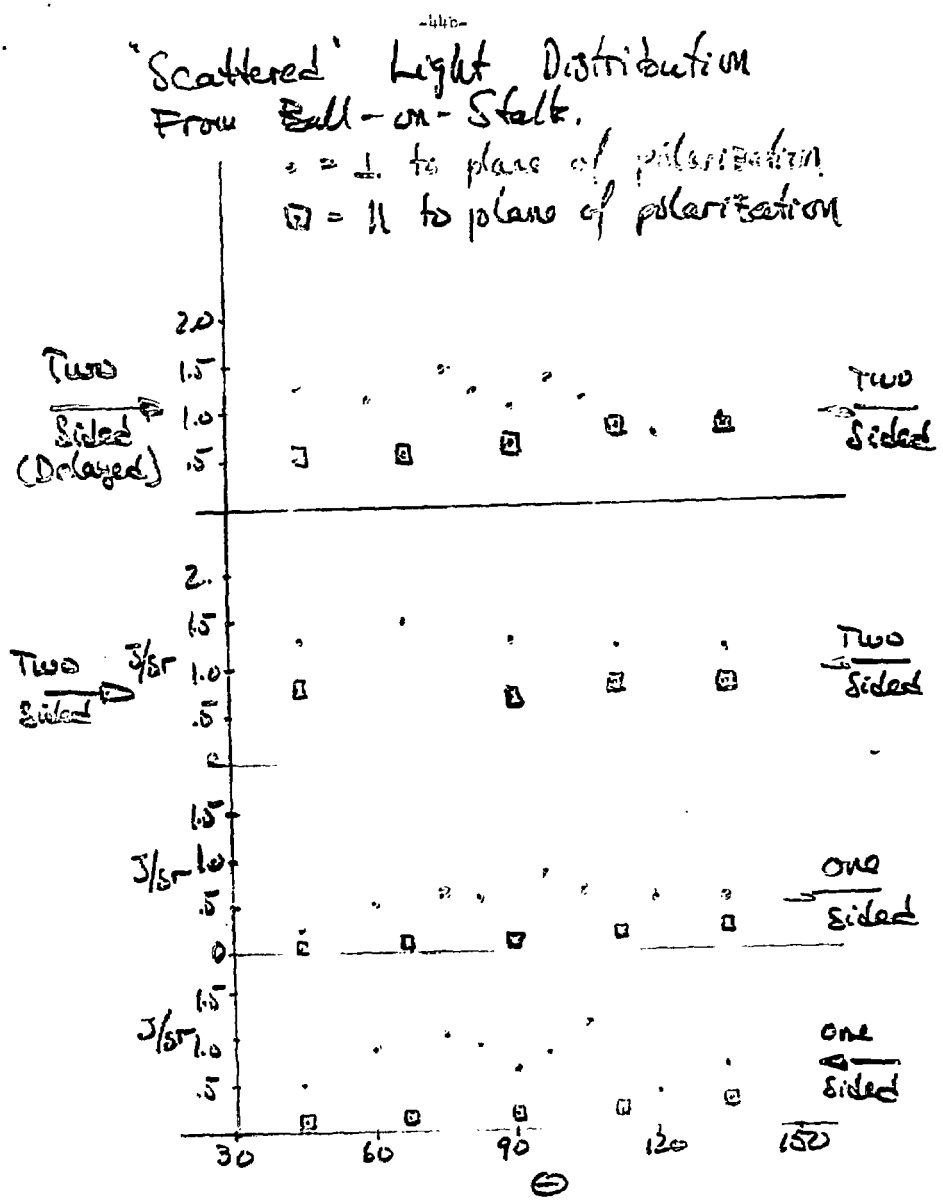
"Scattered" Light Distribution From Ball-on-Stalk.
• = ⊥ to plane of polarization
□ = ∥ to plane of polarization
Two Sided (Delayed)
Two Sided
Two Sided
I/Sr
Two Sided
I/Sr
One Sided
I/Sr
One Sided
2.0
1.5
1.0
.5
2.
1.5
1.0
.5
0
1.5
1.0
.5
1.5
1.0
.5
30
60
90
120
150
θ

X-RAY SPECTRUM VS TARGET SIZE JANUS 2-ARM LASER

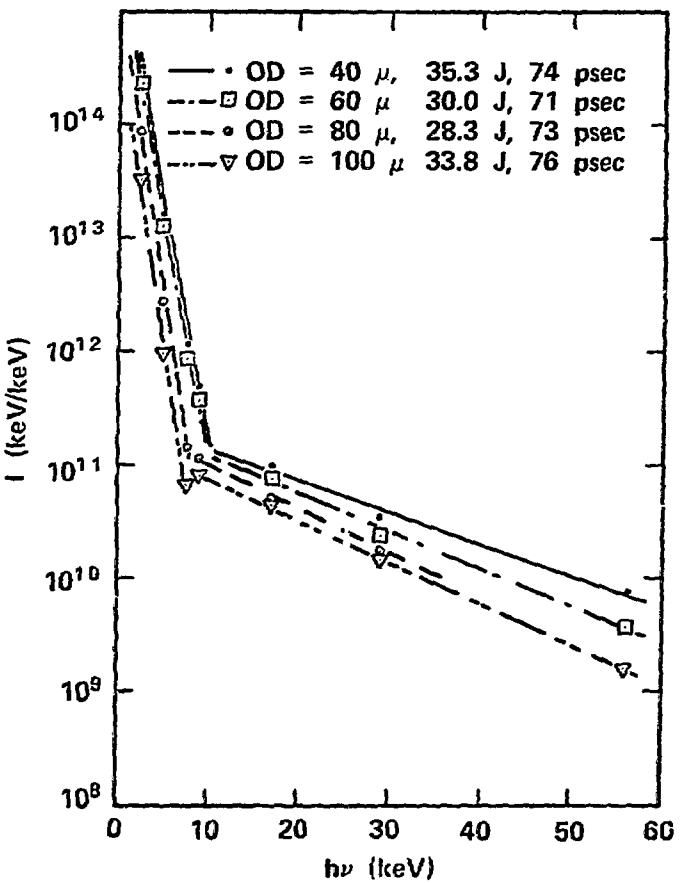

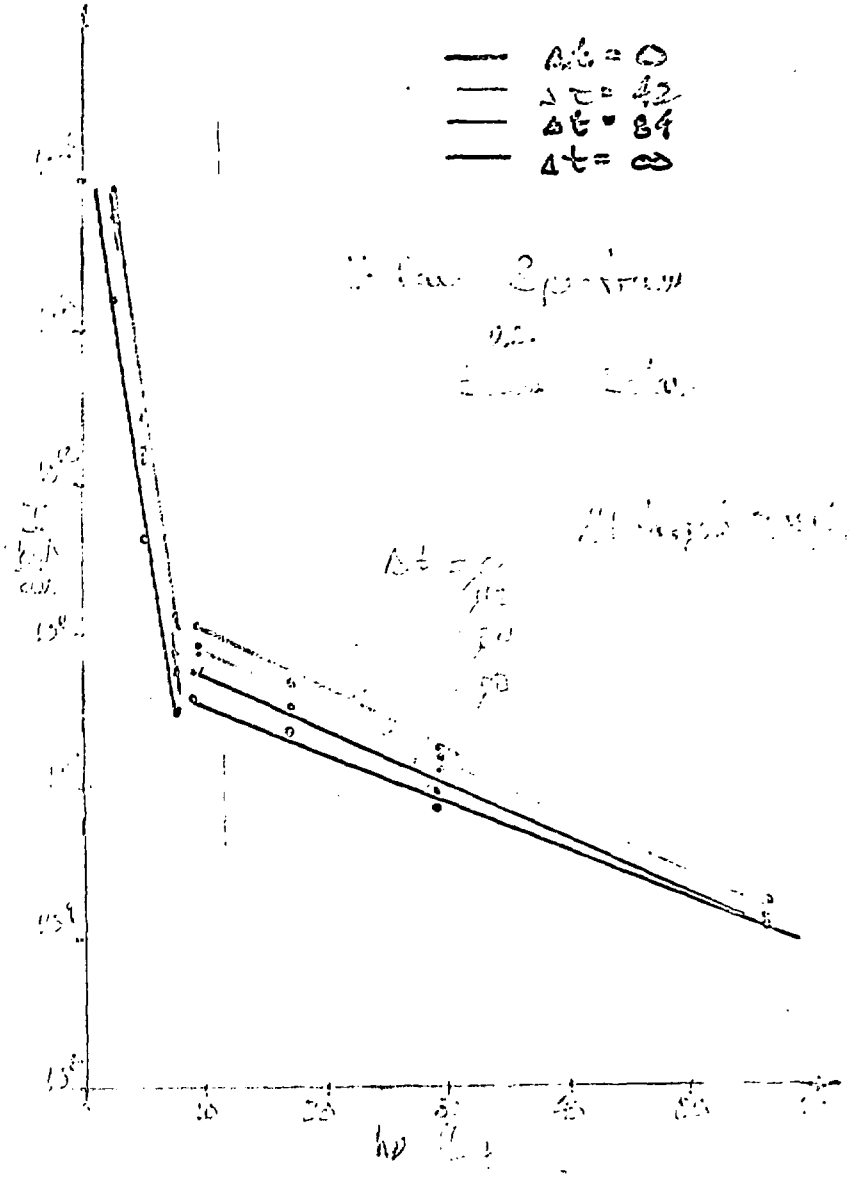

LAGRANGIAN MESH FOR

BALL-ON-STALK TARGET

DT fill = 2 mg/cm^2

Laser energy = 28.3 J

Energy absorbed = 6 J

Laser Pulse FWHM = 73 psec

t = 66 psec after peak of pulse

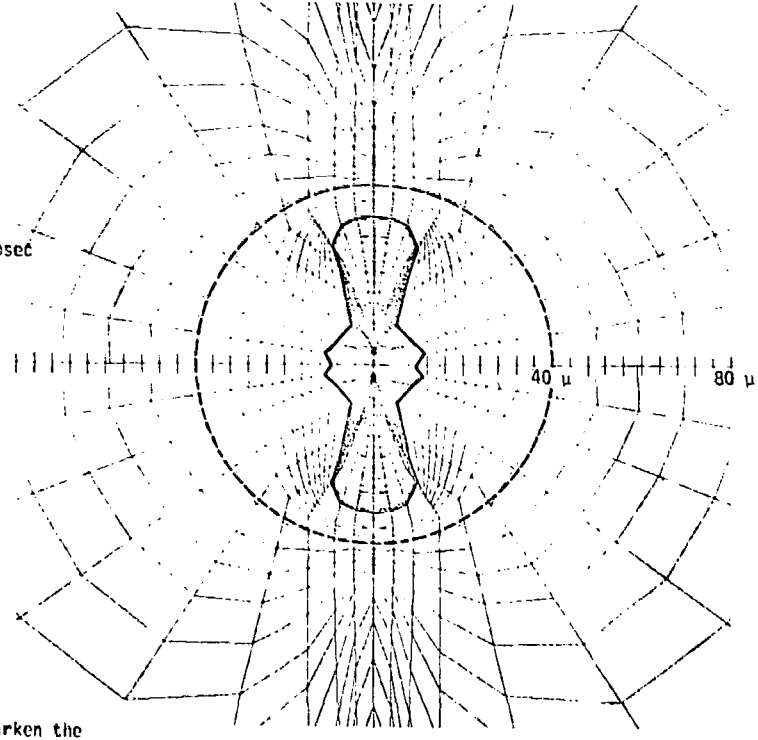

Artist: Please darken the lines. The vugraph is weak on the screen.

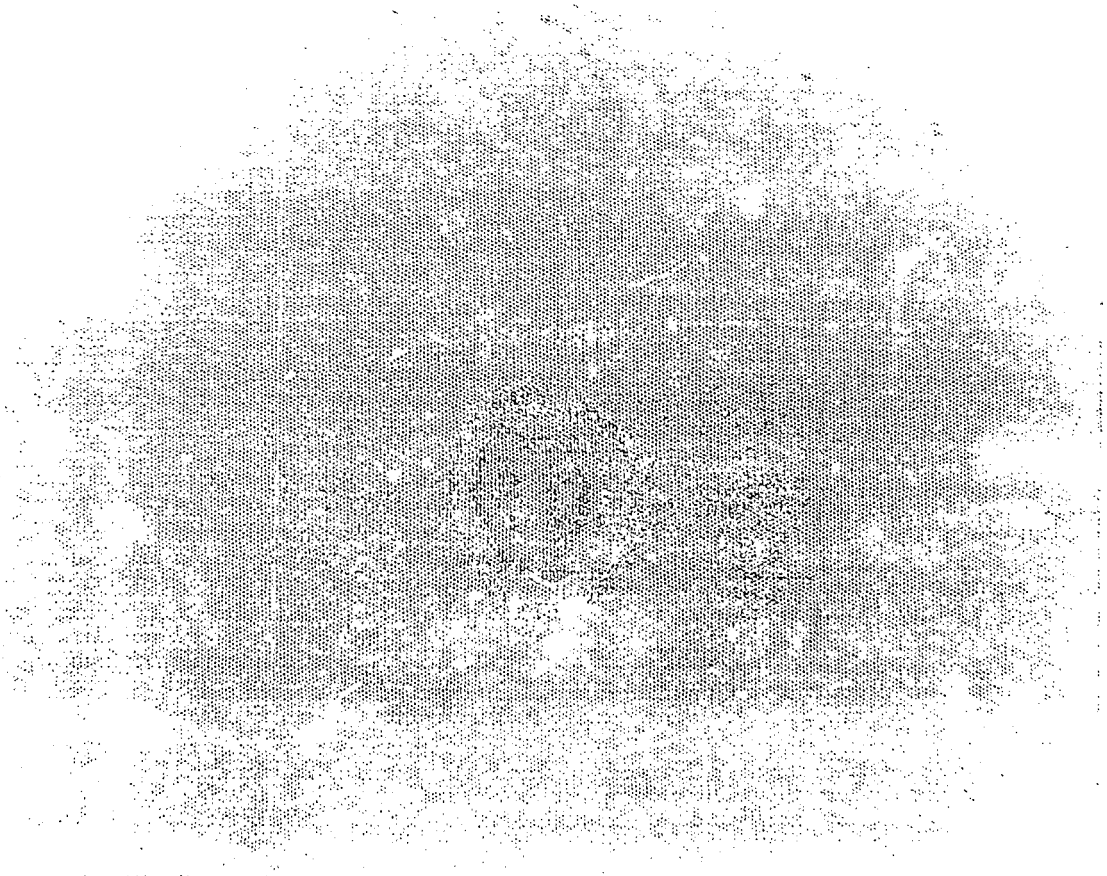

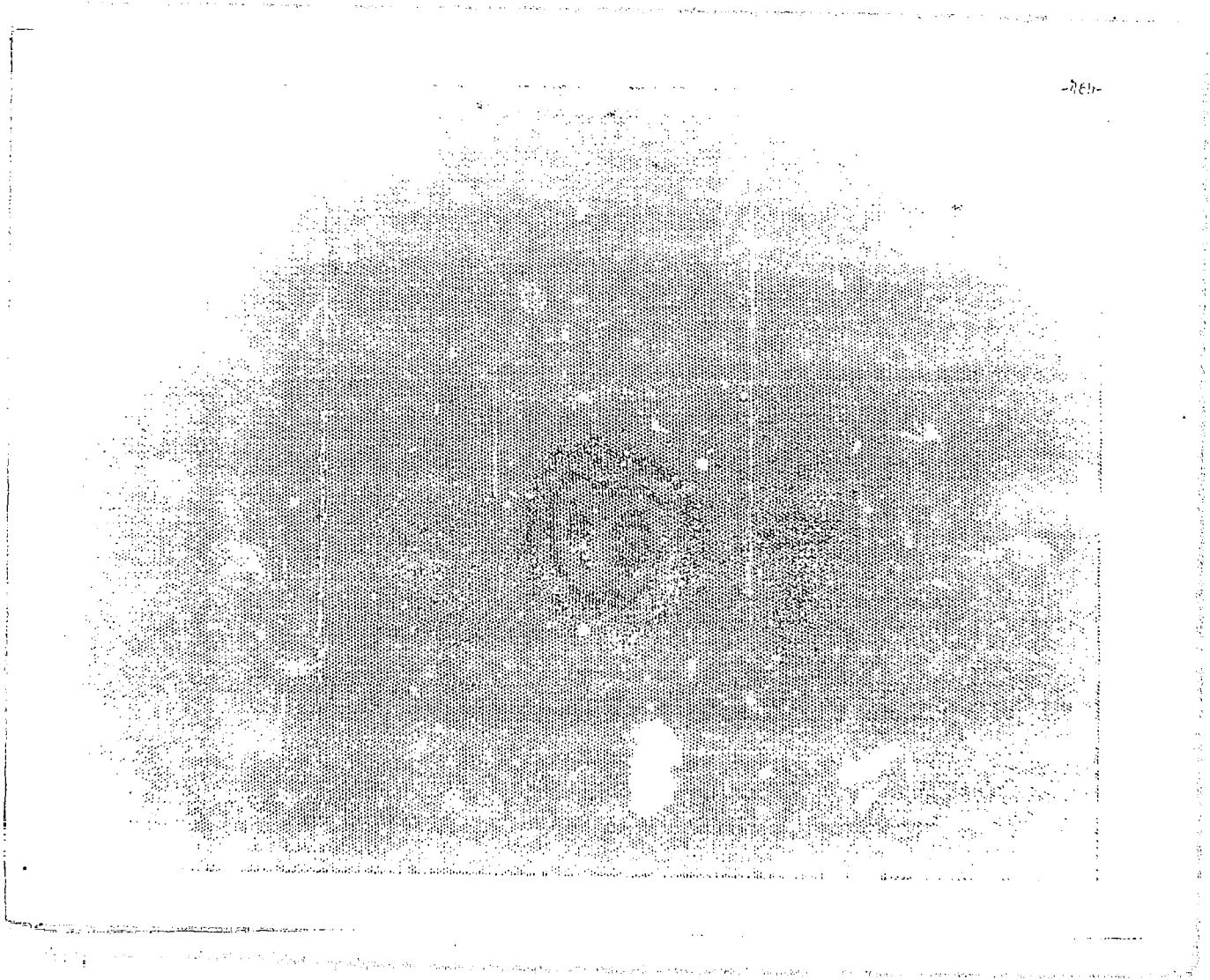

-46-

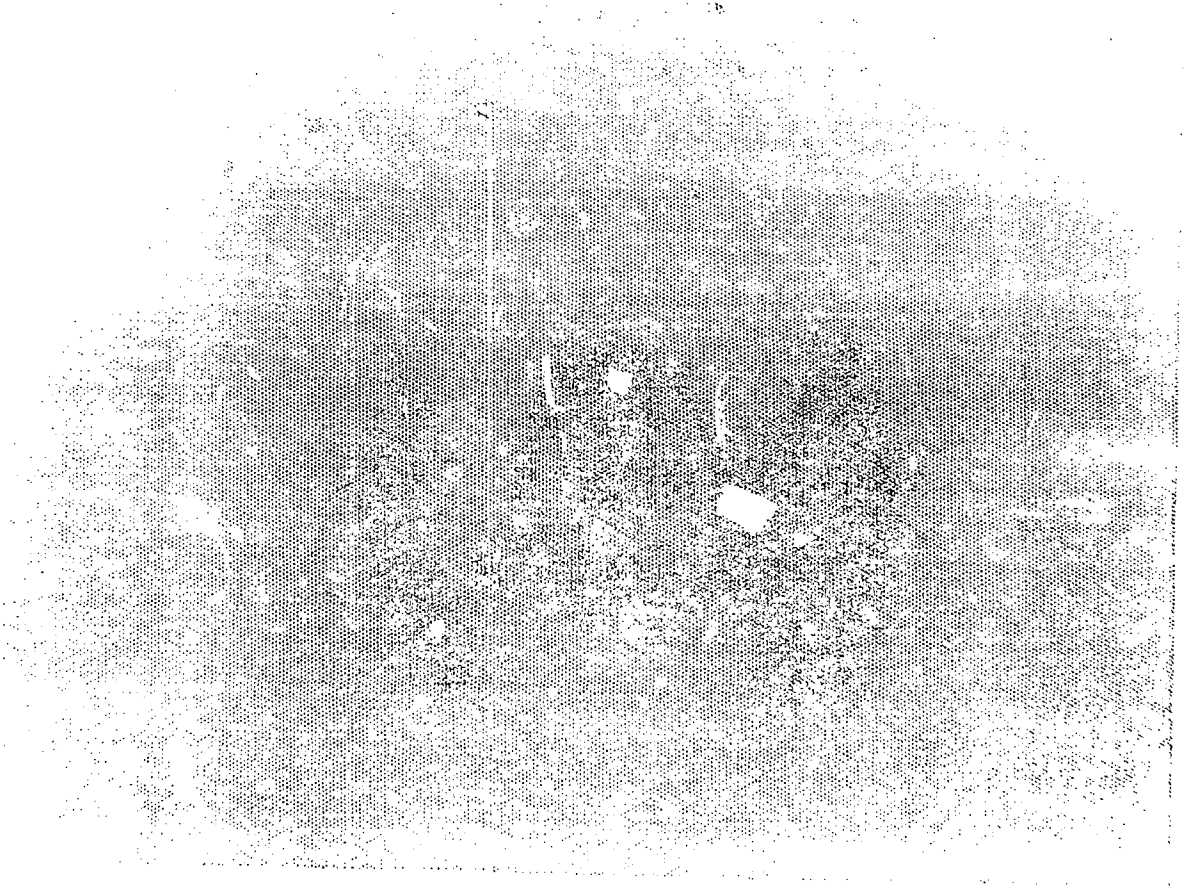

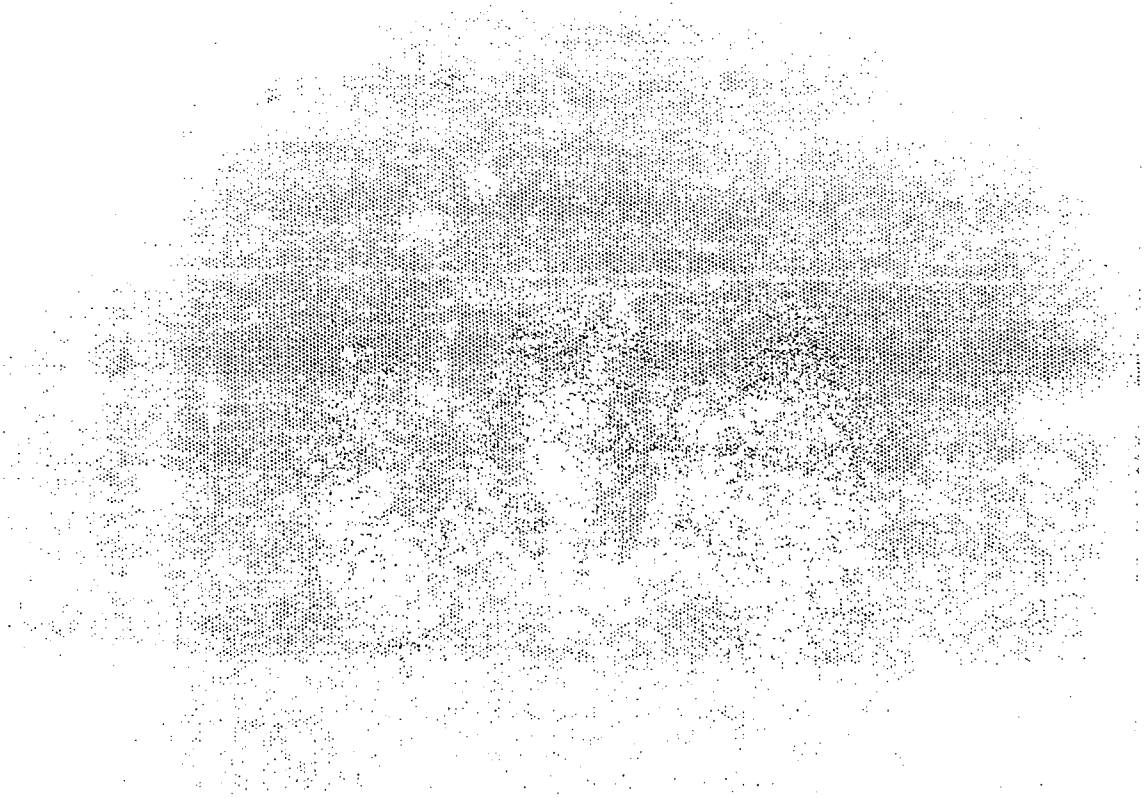

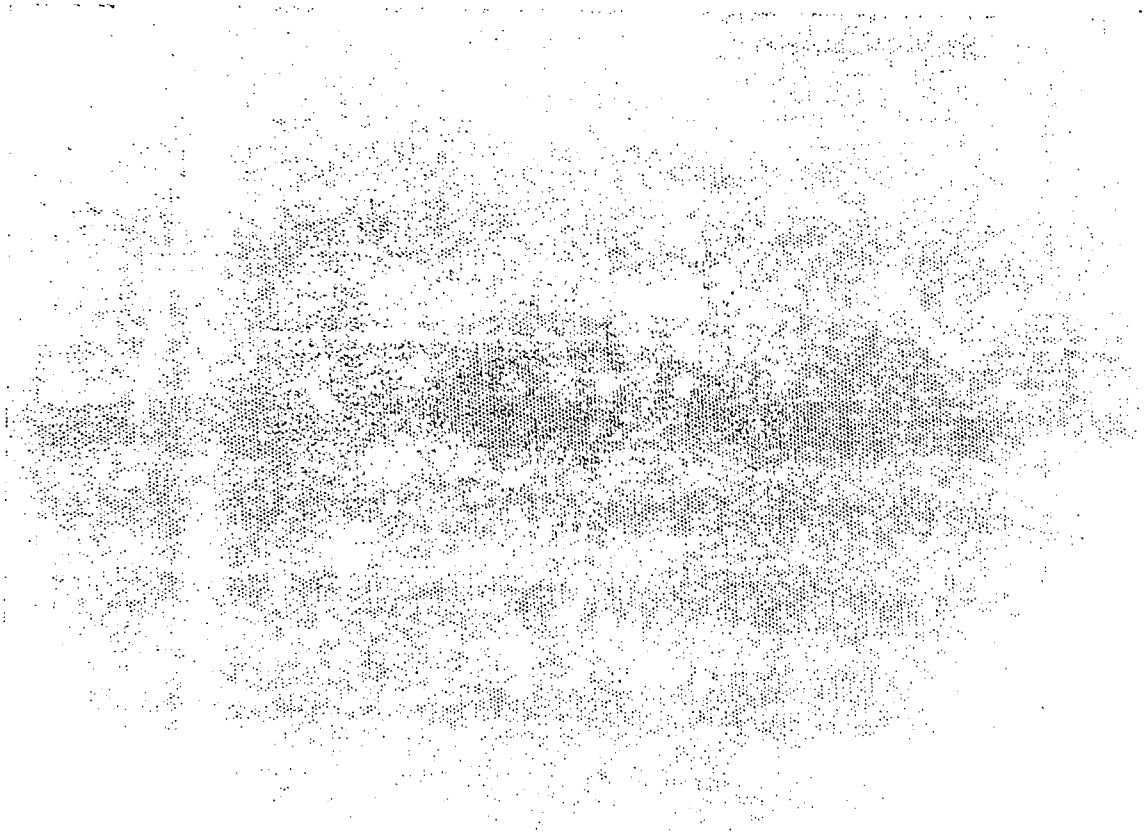

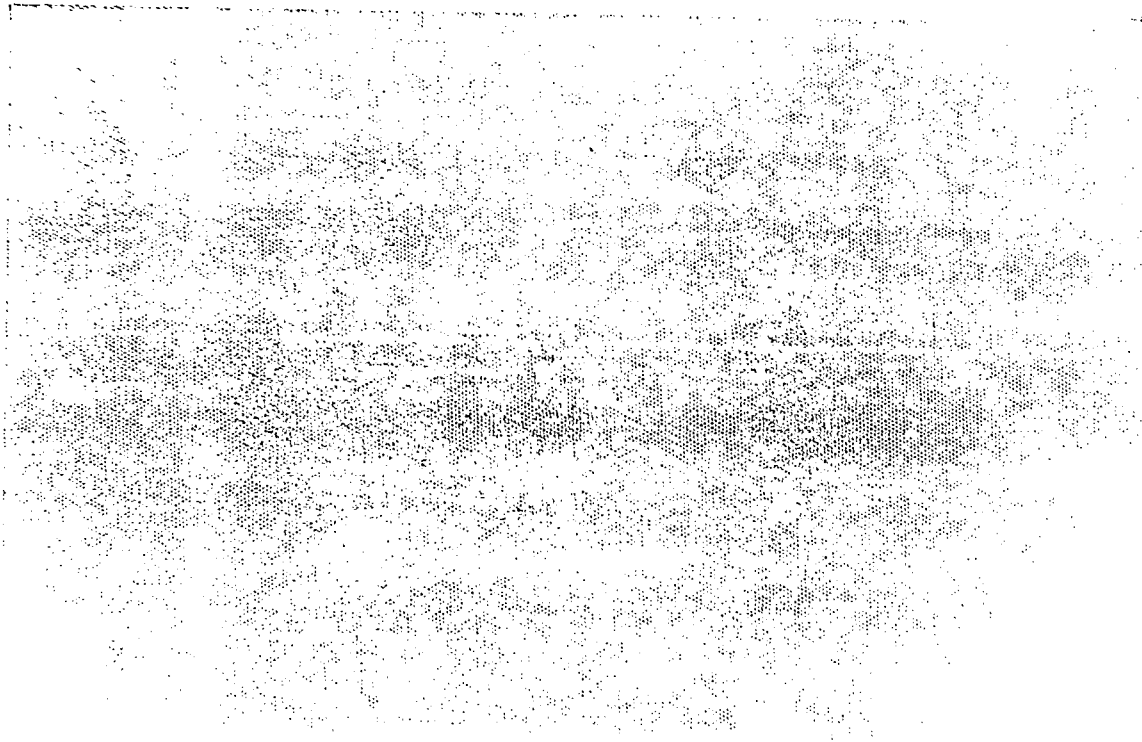

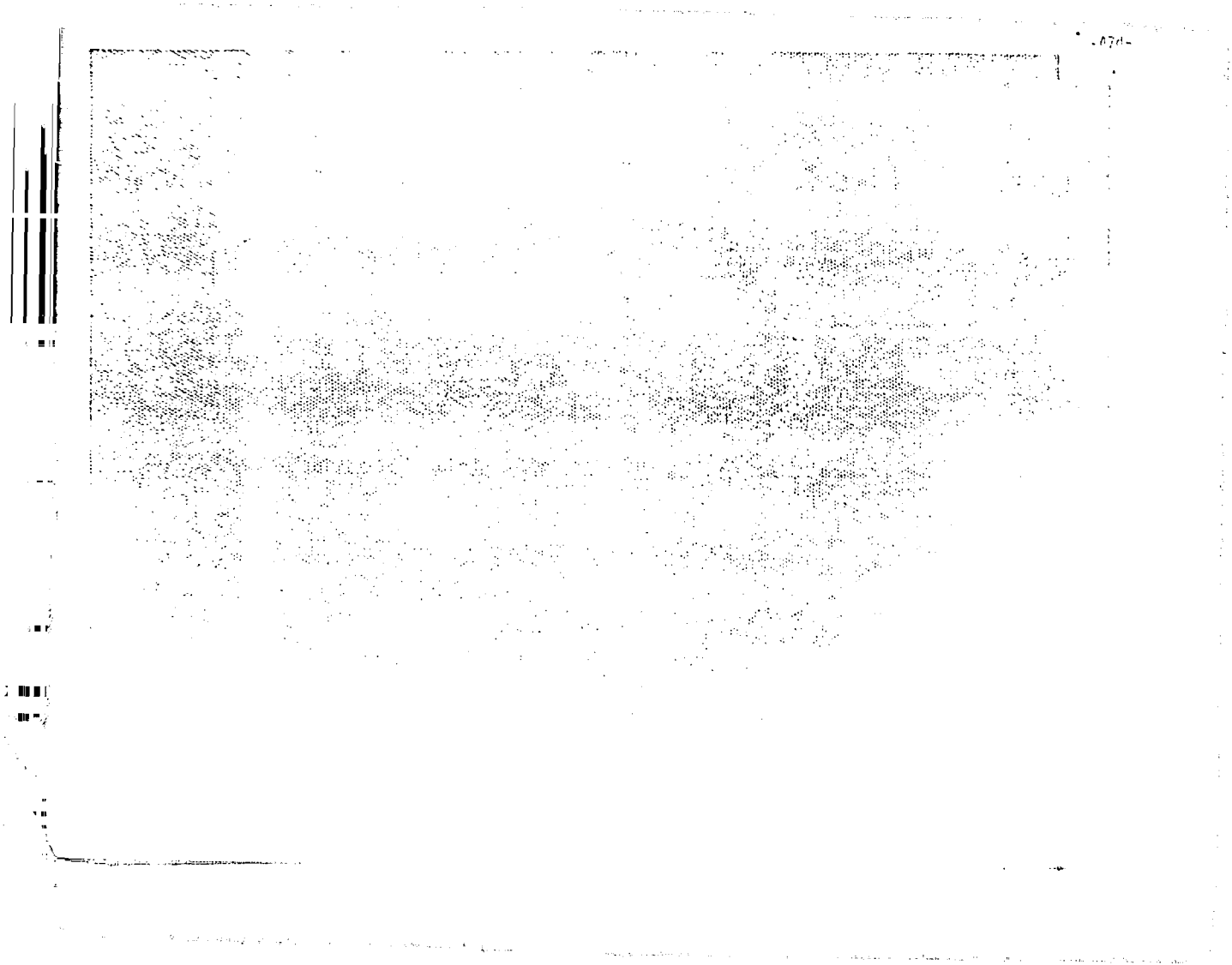

JANUS 2–BEAM B-17 J4 APRIL 24, 1975

Laser energy: East beam – 12.9 J Pulse Neutron
West beam – 13.5 J duration – 62 ps yield – 8.5×10^5

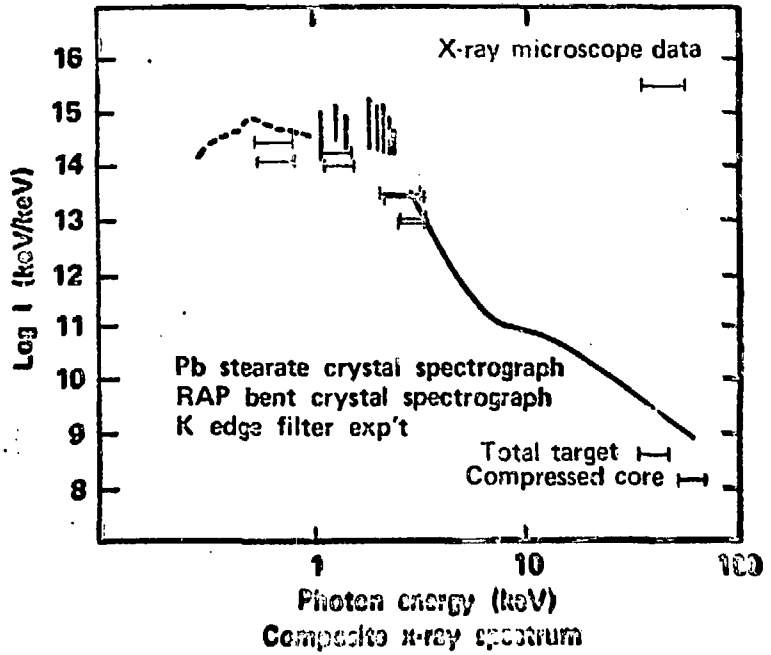

Composite x-ray spectrum

NEUTRONS/JOULES VS JOULES/NG FOR BALL-ON-STALK TARGETS

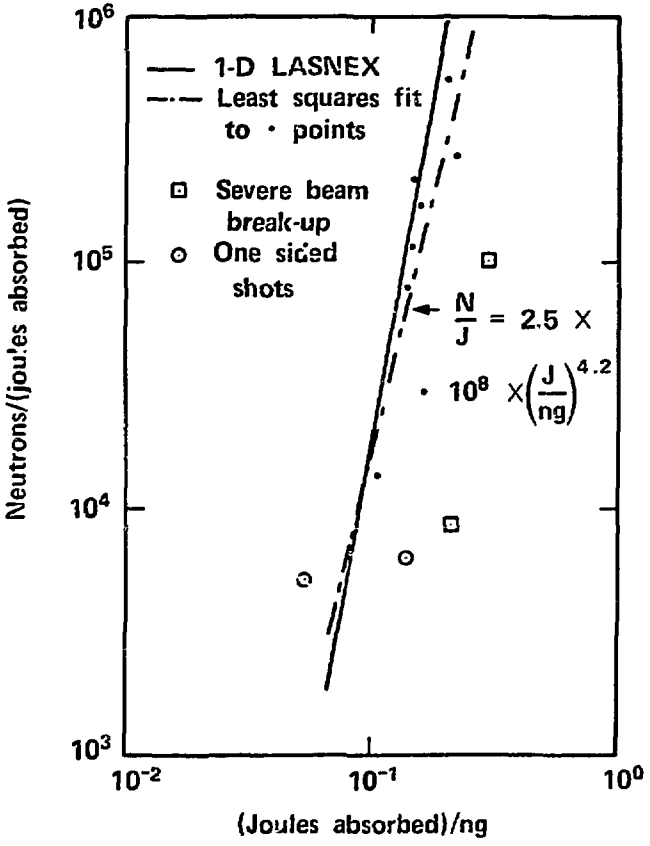

α TOF Spectrometer

Janus II ∿ 400 gigawatt laser

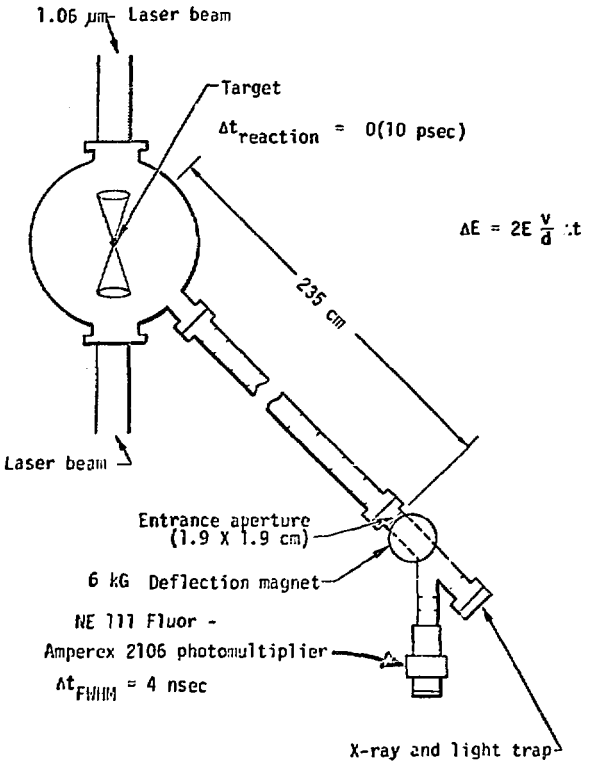

Total flight path = 276.75 cm ⇒ ΔE_{FWHM} = 130 keV

Sensitivity = 5 x 10^{-6} α counts/target reaction

Ti AND E BEAM VS ΔE_{FWHM} OF α

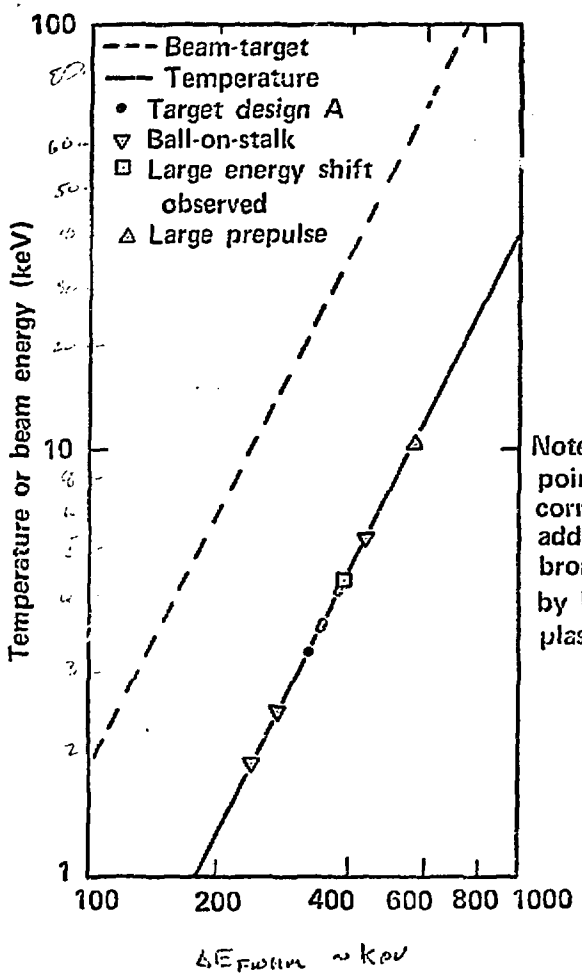

Note: Experimental points are not corrected for additional broadening caused by Doppler and plasma effects.

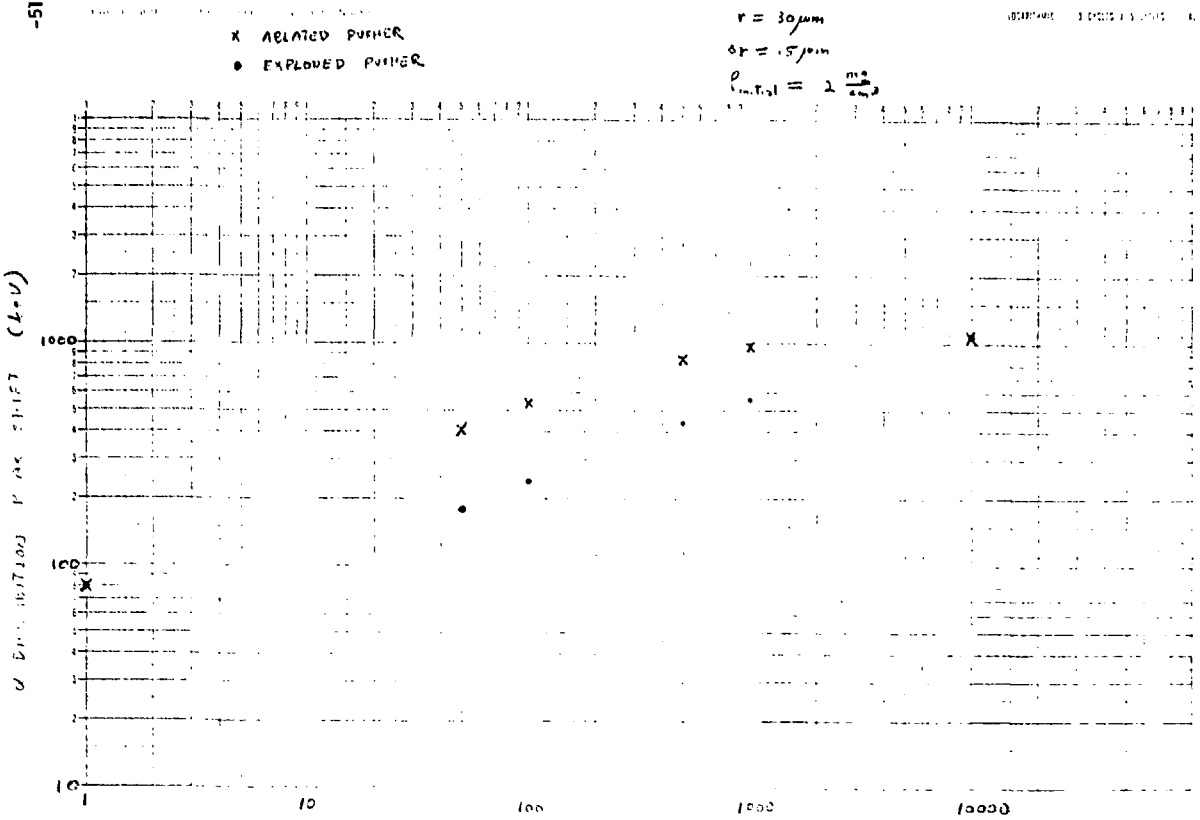
x ABLATED PUSHER
• EXPLODED PUSHER
r = 30 μm
δr = .5 μm
ρ_initial = 2 mg/cm³
1000
100
10
1
10
100
1000
10000

ADDENDUM TO UCRL 77094 Rev 1

LASER FUSION EXPERIMENTS AT THE LAWRENCE LIVERMORE LABORATORY

Harlow G. Ahlstrom

November 3, 1975

Vugraph #1 shows the experimental set up which was used in an attempt to measure the 14.7 MeV protons produced in a fusion reaction of deuterium and helium 3. The purpose of this experiment was further confirmation of the thermonuclear nature of the reactions which we have produced in the implosion of glass microshells filled with fusion fuel. Because of the very large difference in the reaction cross section for DHe^3 reaction as compared to the DT reaction we expected to see a very small number of reactions from the reaction produced from the DHe^3 reactions. Therefore, the method of measuring the reactions was to use nuclear emulsions as the detectors placed very close to the target. The detector was protected from exposure by the x-rays from the target by filters of hafnium and neodymium. A number of experiments were done with typical Livermore laser fusion targets some of which were filled with a 4/4/1 mixture of DHe^3 and tritium. Others were filled with equal molar mixtures of deterium, tritium and $helium^3$. The purpose of having tritium in the targets was to be able to measure the number of nuclear reactions from the deterium tritium reaction by measuring the 14 MeV neutrons and also by measuring the 3.5 MeV alpha particles. Then the measurement of the 14.7 MeV protons from the DHe^3 reaction should agree with the number of neutrons and alphas measured from the DT reaction.

Vugraph #2 shows the ratio of the $\overline{\sigma v}$ for DHe^3 to the $\overline{\sigma v}$ for the deterium tritium reaction as a function of energy or temperature of the plasma. One sees that at temperatures of 1-5 kilovolts the difference in the reaction cross sections is very large and it is this difference that we are attempting to exploit in making this experiment.

Vugraph #3 shows the number of protons that would be seen by the detector as a function of the ion temperature of the reacting plasma or as a function of the potential which either deuterons, tritons or He^3 ions would be accelerated through. The reason for doing the experiment now becomes obvious when one sees that if we have a reaction at an ion temperature of 2 kilovolts, the detector should only see 8 protons. Whereas if the reaction were produced by beam target reaction with a potential of 20 kilovolts the number of protons seen by the detector should be 200. One also sees the discrepancy gets even larger as the potential increases. We have performed a number of these experiments - one of which has been analyzed and the results while not conclusion are supportive of the conclusion that the reaction in the glass microshells are indeed thermonuclear. The number of protons seen by the detector is in the neighborhood of 8 which is in reasonable agreement with the reactions being produced by a Boltzmann distribution and in total disagreement with reactions being produced by an accelerated beam of particles with a potential as low as even 20 kilovolts.

$D + He^3 \rightarrow \alpha + /o$ EXPERIMENT

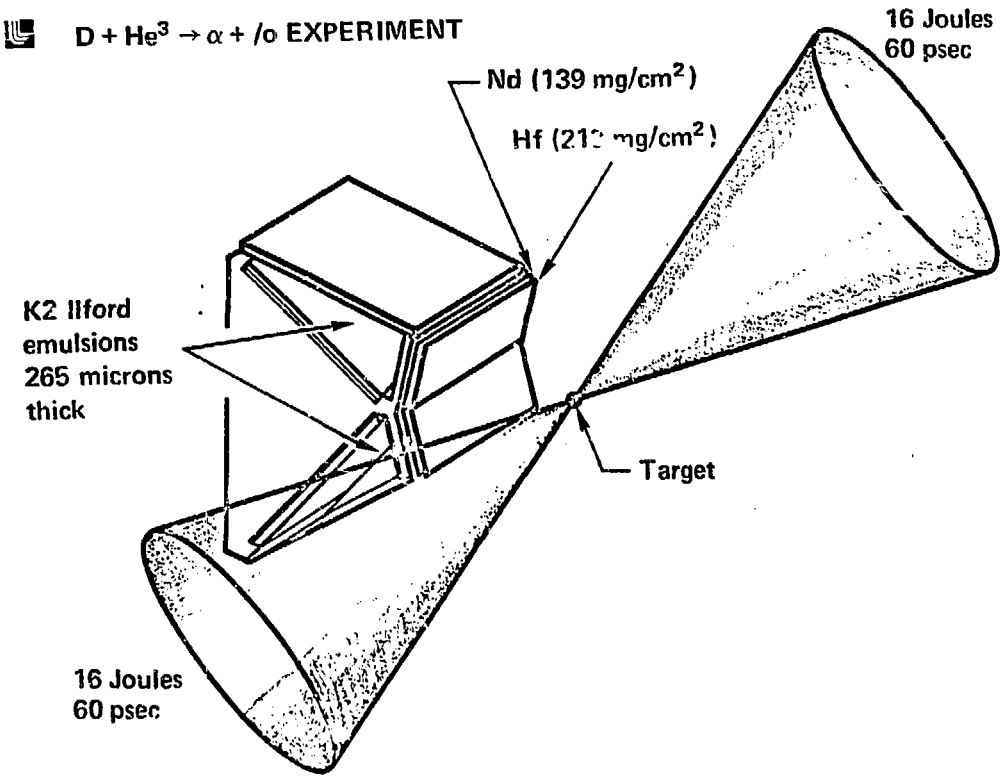

CROSS SECTION RATIOS

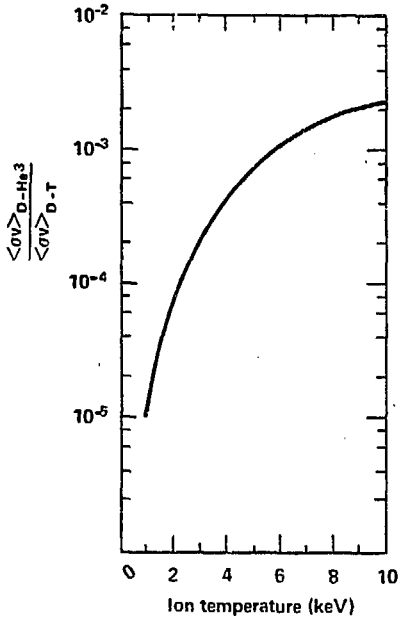

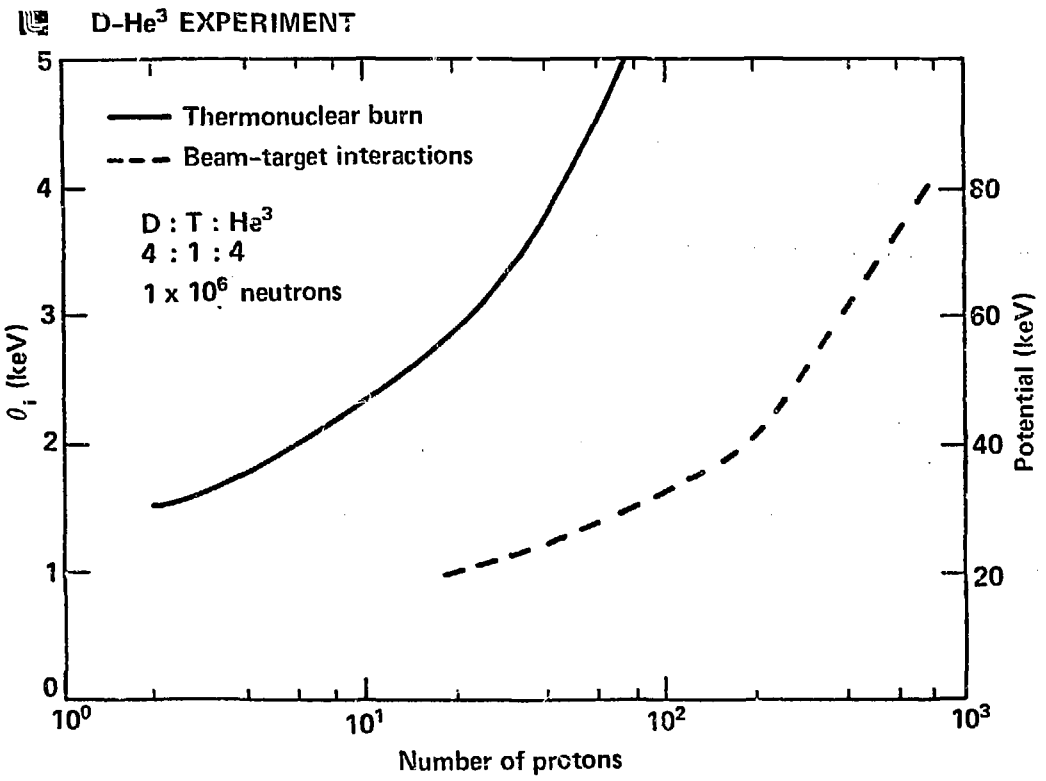
D-He³ EXPERIMENT
Thermonuclear burn
Beam-target interactions
D : T : He³
4 : 1 : 4
1 x 10⁶ neutrons
θ_i (keV)
Potential (keV)
Number of protons
0
1
2
3
4
5
20
40
60
80
10⁰
10¹
10²
10³

ADDENDUM TO UCRL 77094 Rev 1

LASER F SION EXPERIMENTS AT THE LAWRENCE LIVERMORE LABORATORY

Harlow G. Ahlstrom

November 3, 1975

Vugraph #1 shows the experimental set up which was used in an attempt to measure the 14.7 MeV protons produced in a fusion reaction of deuterium and helium 3. The purpose of this experiment was further confirmation of the thermonuclear nature of the reactions which we have produced in the implosion of glass microshells filled with fusion fuel. Because of the very large difference in the reaction cross section for DHe^3 reaction as compared to the DT reaction we expected to see a very small number of reactions from the reaction products from the DHe^3 reactions. Therefore, the method of measuring the reactions was to use nuclear emulsions as the detectors placed very close to the target. The detector was protected from exposure by the x-rays from the target by filters of hafnium and neodymium. A number of experiments were done with typical Livermore laser fusion targets some of which were filled with a 4/4/1 mixture of DHe^3 and tritium. Others were filled with equal molar mixtures of deterium, tritium and $helium^3$. The purpose of having tritium in the targets was to be able to measure the number of nuclear reactions from the deterium tritium reaction by measuring the 14 MeV neutrons and also by measuring the 3.5 MeV alpha particles. Then the measurement of the 14.7 MeV protons from the DHe^3 reaction should agree with the number of neutrons and alphas measured from the DT reaction.

Vugraph #2 shows the ratio of the $\overline{\sigma v}$ for DHe^3 to the $\overline{\sigma v}$ for the deterium tritium reaction as a function of energy or temperature of the plasma. One sees that at temperatures of 1-5 kilovolts the difference in the reaction cross sections is very large and it is this difference that we are attempting to exploit in making this experiment.

Vugraph #3 shows the number of protons that would be seen by the detector as a function of the ion temperature of the reacting plasma or as a function of the potential which either deuterons, tritons or He^3 ions would be accelerated through. The reason for doing the experiment now becomes obvious when one sees that if we have a reaction at an ion temperature of 2 kilovolts, the detector should only see 8 protons. Whereas if the reaction were produced by beam target reaction with a potential of 20 kilovolts the number of protons seen by the detector should be 200. One also sees the discrepancy gets even larger as the potential increases. We have performed a number of these experiments - one of which has been analyzed and the results while not conclusion are supportive of the conclusion that the reaction in the glass microshells are indeed thermonuclear. The number of protons seen by the detector is in the neighborhood of 8 which is in reasonable agreement with the reactions being produced by a Boltzmann distribution and in total disagreement with reactions being produced by an accelerated beam of particles with a potential as low as even 20 kilovolts.

$D + He^3 \rightarrow \alpha + /o$ EXPERIMENT

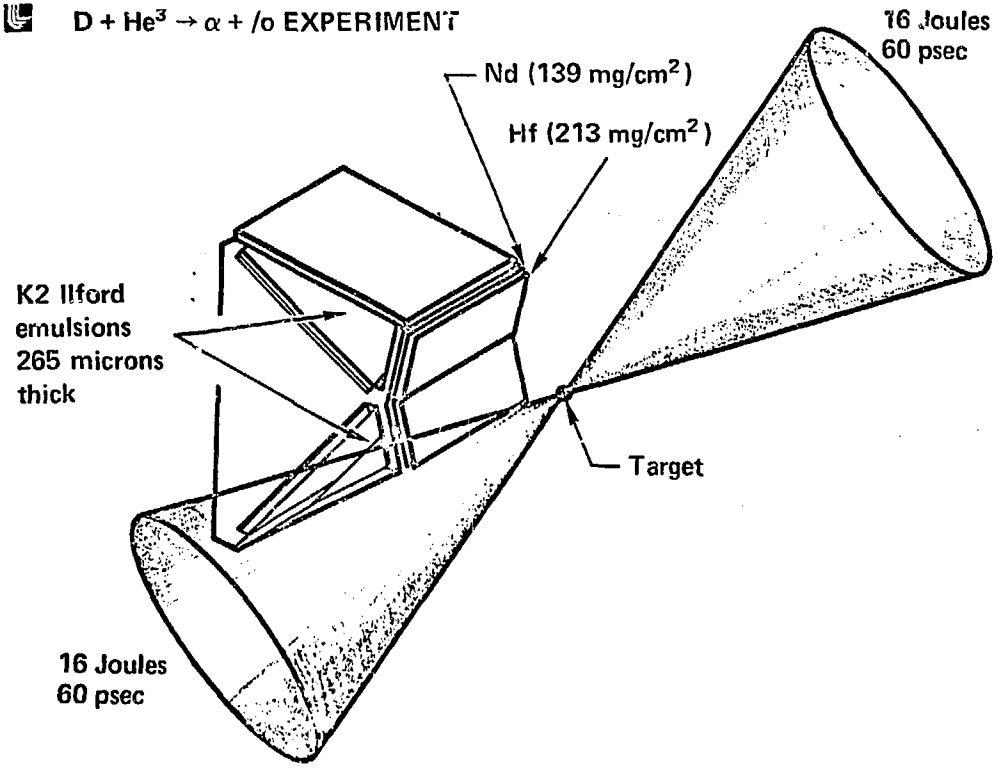

CROSS SECTION RATIOS

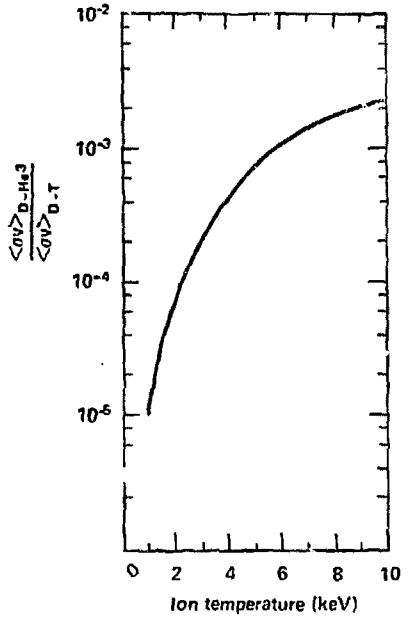

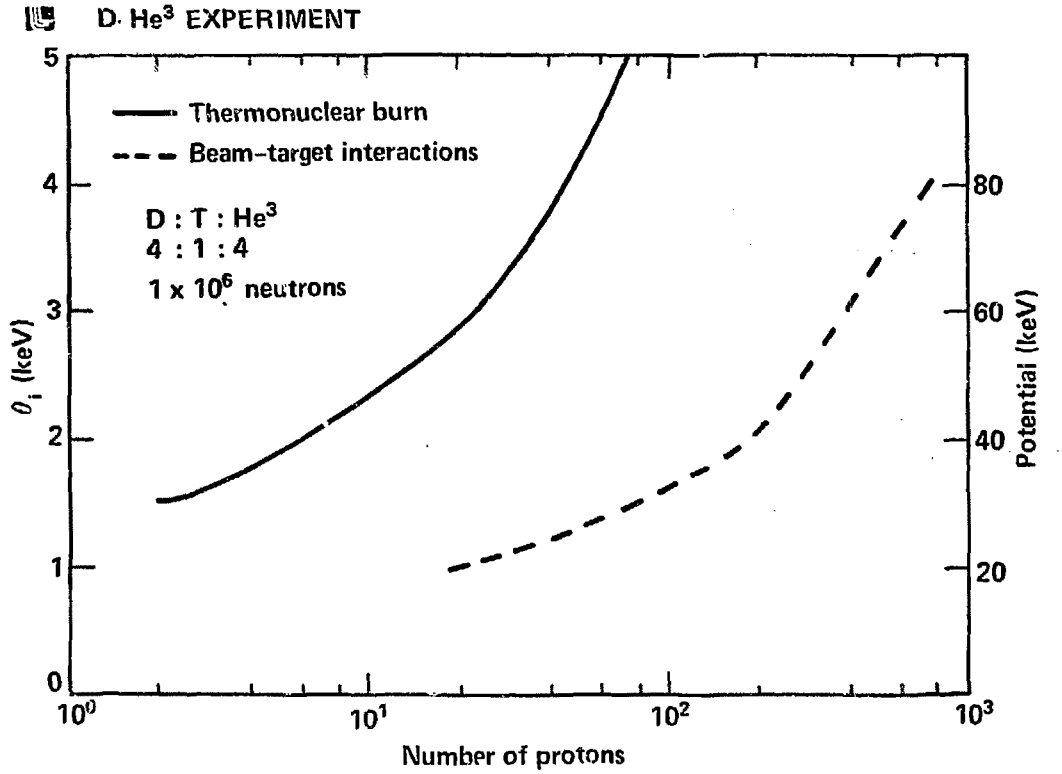
D· He³ EXPERIMENT
Thermonuclear burn
Beam–target interactions
D : T : He³
4 : 1 : 4
1 x 10⁶ neutrons
θi (keV)
Potential (keV)
Number of protons
0
1
2
3
4
5
20
40
60
80
10⁰
10¹
10²
10³